JGR Planets

RESEARCH ARTICLE
10.1029/2020JE006764

A Volcanic Ash Layer in the Nördlinger Ries Impact Structure (Miocene, Germany): Indication of Crater Fill Geometry and Origins of Long-Term Crater Floor Sagging

Gernot Arp[1], István Dunkl[1], Dietmar Jung[2], Volker Karius[1], Réka Lukács[3], Lingqi Zeng[1], Andreas Reimer[1], and James W. Head III[4]

[1]Geoscience Center, Georg-August-University, Göttingen, Germany, [2]Geological Survey, Bavarian Environment Agency, Hof/Saale, Germany, [3]MTA-ELTE Volcanology Research Group, Budapest, Hungary, [4]Department of Earth, Environmental and Planetary Sciences, Brown University, Providence, RI, USA

Key Points:

- A critical question in the evolution of impact-crater-hosted lakes is the origin and timing of post-impact floor subsidence
- We describe a volcanic ash layer from the Ries impact crater that demonstrates a deeply bowl-shaped geometry of its lacustrine crater fill
- This geometry, leading to a concentric outcrop pattern, requires significant crater floor sagging, in addition to sediment compaction

Supporting Information:

Supporting Information may be found in the online version of this article.

Correspondence to:

G. Arp,
garp@gwdg.de

Citation:

Arp, G., Dunkl, I., Jung, D., Karius, V., Lukács, R., Zeng, L., et al. (2021). A volcanic ash layer in the Nördlinger Ries impact structure (Miocene, Germany): Indication of crater fill geometry and origins of long-term crater floor sagging. *Journal of Geophysical Research: Planets*, *126*, e2020JE006764. https://doi.org/10.1029/2020JE006764

Received 6 NOV 2020
Accepted 5 MAR 2021

Abstract Since its recognition as an impact structure 60 years ago, no volcanics were anticipated in the circular depression of the 14.8 Ma old Nördlinger Ries. Here, we describe for the first time a volcanic ash-derived clinoptilolite-heulandite-buddingtonite bed within the 330 m thick Miocene lacustrine crater fill. Zircon U-Pb ages of 14.20 ± 0.08 Ma point to the source of the volcanic ash in the Pannonian Basin, 760 km east of the Ries. The diagenetically derived zeolite-feldspar bed occurs in laminated claystones of the Ries soda-lake stage and represents the first unequivocal stratigraphic marker bed in this basin, traceable from marginal surface outcrops to 218 m below surface in the crater center. These relationships demonstrate a deeply bowl-shaped geometry of crater fill sediments, not explainable by sediment compaction and corresponding stratigraphic backstripping alone. Since most of the claystones formed at shallow water depths, the bowl-shaped geometry must reflect 134 +23/−49 m of sagging of the crater floor. We attribute the sagging to compaction and closure of the dilatant macro-porosity of the deeply fractured and brecciated crater floor during basin sedimentation and loading, a process that lasted for more than 0.6 Myr. As a result, the outcrop pattern of the lithostratigraphic crater-fill units in its present erosional plane forms a concentric pattern. Recognition of this volcanic ash stratigraphic marker in the Ries crater provides insights into the temporal and stratigraphic relationships of crater formation and subsidence that have implications for impact-hosted lakes on Earth and Mars.

Plain Language Summary We describe for the first time a volcanic ash layer from the lake sediment fill of the 14.8 million years old asteroid impact crater Nördlinger Ries. Radiometric age and trace element characteristics of this ash layer are identical to that of a volcanic field in Hungary, so that the ash reflects a volcanic eruption 760 km east of the Ries basin. Recognition of this ash layer enables its use as a marker bed. The ash layer can be traced from surface outcrops to 218 m depth in drillings. This indicates that the strata are significantly inclined toward the crater center. Calculations of sediment compaction by further sediment load and burial only partially explain the observed deeply bowl-shaped geometry. We attribute the additional sagging to the subsidence of the crater floor substrate, formed of rocks highly shattered by the impact event. Both effects cause a concentric pattern of outcropping strata in the partially eroded crater fill. The presence of the ash layer and its use to help disentangle the source and timing of subsidence (due to compaction of lake sediments, and closure of deeper, impact-induced fractures), has important implications for lakes formed in impact craters on Earth and Mars.

1. Introduction

The stratigraphy and sedimentary environments of impact crater interior sedimentary fill form valuable climate archives on Earth, in particular those in young impact structures such as Bosumtwi and El'gygytgyn. Only a few terrestrial impact structures with preserved sedimentary fill are known. These are primarily present-day crater lakes such as Pingualuit, Bosumtwi, El'gygytgyn, and Tswaing (Guyard et al., 2011; Melles et al., 2012; Partridge et al., 1993; Shanahan et al., 2009; Talbot & Johannessen, 1992). These crater fill deposits precisely record Quaternary climate changes, such as aridification or glacial cycles, as revealed by geochemistry, stable isotopes, and palynomorphs (Melles et al., 2012; Shanahan et al., 2009; Talbot & Johannessen, 1992). Fossil examples, however, are commonly buried (Boltysh: Gurov et al., 2006; Chesapeake

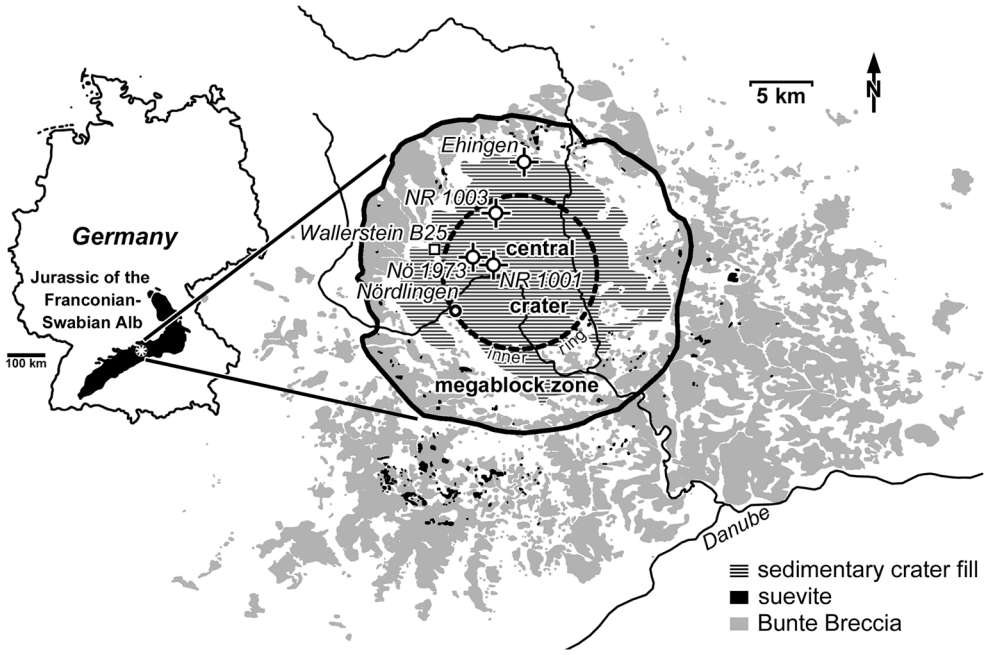

Figure 1. Location of the outcrop Wallerstein B25, the investigated drillings NR 1001, NR 1003, Nö 1973, Ehingen, and major structural elements of the Ries impact structure (based on Ernstson, 1974; Hüttner & Schmidt-Kaler, 1999; Pohl et al., 1977).

Bay: Gohn et al., 2008) or significantly eroded (Steinheim: Reiff, 1977; Haughton: Osinski et al., 2005). In a similar manner, lacustrine crater fill deposits on Mars potentially form archives of the climatic development throughout Mars history, and particularly during the Noachian-Hesperian climate transition, when Mars changed from at least episodically warm to the current extremely cold and arid conditions (for review see e.g. Carr & Head, 2010a, 2010b; Craddock & Howard, 2002; Fassett & Head, 2008a, 2008b; Grotzinger & Milliken, 2012; Goudge et al., 2015, 2016; Irwin et al., 2005; Milliken et al., 2010). We report here on the discovery and documentation of a volcanic-ash derived marker bed in the Nördlinger Ries impact structure that we use to outline the nature of the subsidence history of the crater lake floor, and the origin and timing of the observed bowl-shaped crater fill geometry with significantly inclined strata. We explore some implications for the history of other crater lakes on Earth and Mars.

2. The Nördlinger Ries Structure and Stratigraphy

The Nördlinger Ries is a 14.808 ± 0.038 Ma old (Middle Miocene) (Schmieder et al., 2018a; for discussion see Rocholl, Böhme, et al., 2018; Rocholl, Schaltegger, et al., 2018 and Schmieder et al., 2018b), partially exhumed impact crater, structurally subdivided into a central crater, an inner ring, and a marginal block zone delineated by the tectonic crater rim (Figure 1; Pohl et al., 1977). The impact occurred in volatile-rich target rocks (Artemieva et al., 2013; Osinski, 2004, 2006). Two ejecta blankets are distinguished: 1) the Bunte Breccia (showing a rampart structure; Sturm et al., 2013) and 2) the overlying impact-melt bearing suevite (Hüttner, 1969; Stöffler et al., 2013; Siegert & Hecht, 2019; Siegert et al., 2017; von Engelhardt, 1997). By the end of the Miocene (~5.33 Ma), the Ries crater was completely covered by sediments (Schröder & Dehm, 1950), and subsequently, Plio- to Pleistocene erosion removed about 100 m of sediment within the crater as well as parts of the ejecta blankets (Hüttner, 1969; Wolf, 1977). The sedimentary fill preserved today consists of four lithostratigraphic units (Jankowski, 1977a, 1981):

(i) The basal member: Consists of conglomerates and sandstones derived from suevite and crystalline basement rocks, with intercalated playa deposits
(ii) The laminite member: Comprised of laminated marls and bituminous shales, with authigenic silicates (analcime, clinoptilolite) and abundant slumping structures

(iii) The marl member: Characterized by stratified calcareous claystones and poorly bedded dolomitic marls. These are partially bioturbated and contain analcime only sporadically
(iv) The clay member: The youngest preserved unit consists of an alternation of clays, marls and limestones, with intercalated carbonaceous clays, lignites, and gypsum-pseudomorph-bearing limestones

While these units can be recognized in drill cores of the central crater basin, sections in marginal positions (short drill cores, rotary drillings, and temporary exposures) are more difficult to assign to specific units. Therefore, the surface outcrop pattern of these units, the basin-center to basin-margin correlations, and consequently, the crater fill geometry, has remained poorly constrained and a matter of controversy in the literature (Arp et al., 2013; Jankowski, 1981; Schauderna, 1983; Wolff & Füchtbauer, 1976). The volcanic-ash derived marker bed that we describe here was discovered in a temporary exposure during the construction of a state road B 25 underpass in the western Ries basin near Wallerstein (Figure 1; Text S1). Subsequently, the same bed was found in a percussion drill core at northern Ries basin margin (Ehingen-SE), and in three drill cores from the basin center (Figure 1; Text S1). We outline the characteristics and distribution of this volcanic-ash-deposited marker bed and use these data to help constrain the filling and subsidence history of the Nördlinger Ries crater lake.

3. Materials and Methods

Five samples of the outcrop Wallerstein B25, three samples of the drill cores Nördlinger Ries 1001, 1003 and Nördlingen 1973, 22 samples of percussion drill core Ehingen-SE, one sample from Ehinger Bach (Figure 1), and five reference samples from the Northern Alpine Foreland Basin and the Leinetal Graben have been investigated (Text S2 and Data Set S1).

The mineralogical composition (Text S2) was analyzed by powder X-ray diffraction using a Philips PW 1800 diffractometer operating at 45 kV and 40 mA with monochromated Cu Kα radiation. The range 4°2θ–70°2θ was scanned with a step width of 0.02°2θ. The counting time was 3 s per step. Mineral identification was carried out using the X'Pert High-Score Plus software (PANalytical). Quantification of mineral phases was performed by Rietveld calculations using the program AutoQuant.

The elemental composition of the samples (Data Set S1) was determined by X-ray fluorescence analysis (PANalytical Axios Advanced XRF spectrometer fitted with a 4 kW Rh anode SSTmAx X-ray tube) on glass fusion disks. Samples with high S and C_{org} contents were previously heated at 650°C for 3 h in a furnace. Total carbon, nitrogen, and sulfur were analyzed with a Euro EA 3000 Elemental Analyzer (Hekatech, Wegberg, and Germany) applying BBOT (2.5-Bis [5-tert-benzoxazol-2-yl] thiophene) and atropine sulfate monohydrate (IVA Analysetechnik, Meerbusch, Germany) as reference materials. Organic and inorganic carbon content was separated using a gradual heating method on a LECO RC612 multi-phase carbon analyzer (Leco, St Joseph, MI, USA), calibrated against LECO carbon standards (1.00%C, 4.98%C, and 12.00%C).

Laser ablation ICP-MS U-Pb dating of the volcanogenic zircon crystals was performed in the GÖochron Laboratories of University of Göttingen. The details of the laboratory procedure is in the Text S3 and Data Set S2.

Modeling of compaction and stratigraphic backstripping (Data Set S3 and S4) was calculated on basis of the Athy equation (Athy, 1930; Sclater & Christie, 1980), modified by Maillart (1991):

$$\varphi_Z = \varphi_{res} + \left(\varphi_0 - \varphi_{res}\right) e^{-\alpha z \beta},$$

with ϕ_0 = porosity at time of deposition, ϕ_z = porosity at burial depth z (m), ϕ_{res} = residual porosity, and α and β empirical compaction coefficients. The reason for using the modified equation is that the Maillart equation introduces a "residual porosity" ϕ_{res} to account for remaining porosities at greater depths (see e.g., Einsele, 2000; Revil et al., 2002), and an additional coefficient β, which is required for a fitting to measured porosities at near surface depth (specifically during early dewatering of laminites). The curve for pelitic sediments (Figure 2) was aligned to measured porosities in laminites of the drill core Nördlingen 1973 (Jankowski, 1977a) and porosities in surface sediments of Lake Van (Data Set S3; Landmann et al., 1996 and Reimer et al., 2009) by modifying the empirical compaction coefficients α and β. The varved Lake Van

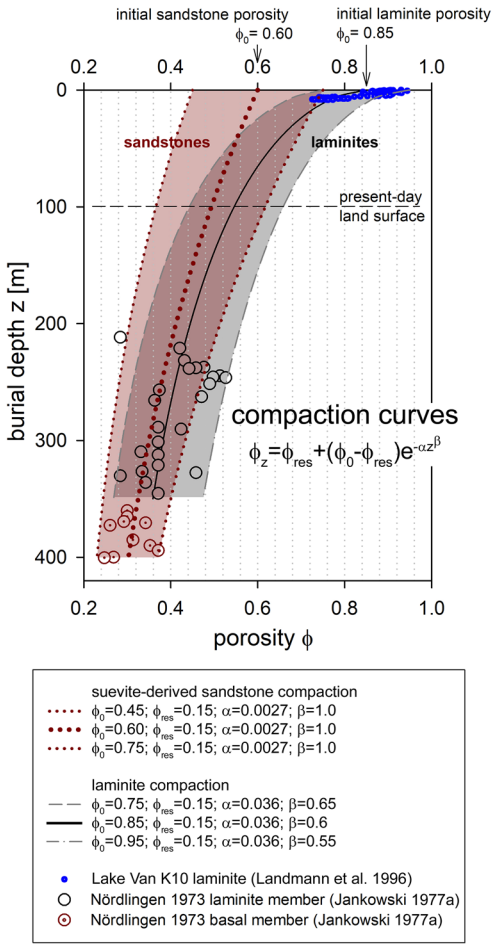

Figure 2. Compaction curves used in this study for back-stripping the position of the volcanic-ash-derived zeolite-feldspar bed in the Ries Crater Lake. For calibration, porosity data of Jankowski (1977a) and Landmann et al., (1996) were used. For details of calculations see Data Set S3.

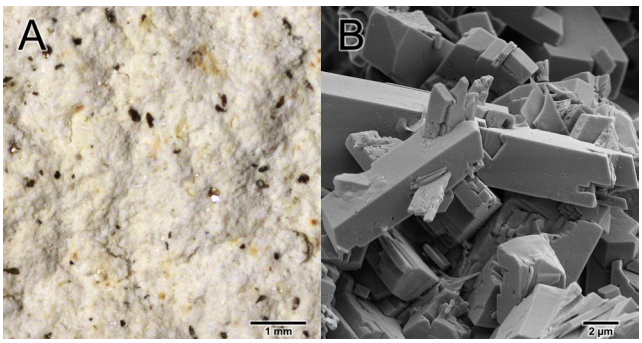

Figure 3. (a) Basal part of the volcanic-ash derived zeolite bed at Wallerstein B 25, showing black biotite crystals within a zeolite matrix. (b) Scanning electron micrograph of the same sample showing monoclinic clinoptilolite-heulandite crystals.

sediments (Landmann et al., 1996; Stockhecke et al., 2014) are similar to the laminites of the Ries (Bolten et al., 1976; Jankowski, 1981; Weber, 1941) with respect to carbonate contents and lamination (alternation of light carbonate-rich, and dark C_{org}– and clay-rich laminae; similar laminae thickness). As a measure for uncertainty, the compaction was also calculated for ±10% initial porosity (at $z = 0$). The compaction curve for sandstones (Figure 2) was calculated in the same way, with an initial porosity of 0.60, that is, intermediate between 0.45 for pure sand (Beard & Weyl, 1973) and the very high value of 0.75 as used e.g. in Kominz and Pekar (2001). The ratio of present-day ϕ_z and ϕ_z at the time of zeolite bed deposition was used for stratigraphic backstripping of the sediment column below the zeolite bed, subdivided in 1 m thick intervals. The surface distribution pattern of lithofacies units was compiled from percussion corings, diploma thesis mapping, unpublished and published drilling reports, and data from the drill database BIS Bayern (Data Set S5).

4. Results

4.1. Composition, Age and Source of the Volcanic Ash

Construction of the Wallerstein B25 state road underpass in the western Ries basin (Figure 1) exposed, at 440 m a.s.l., a 14 cm thick white porous and light zeolite bed intercalated between aragonite-bearing laminites. Quantitative XRD analyses demonstrate that the zeolite bed largely consists of clinoptilolite (63 wt%) and heulandite (34 wt%), with only traces of other minerals (quartz). The zeolite bed shows a 2 cm thick graded basal layer, with clinoptilolite (45 wt%), heulandite (29 wt%), smectite (8 wt%), plagioclase, quartz, muscovite and biotite. Allanite and zircon were found in the heavy mineral fraction. The black, idiomorphic biotite crystals display a grain-size gradation within the basal layer (Figure 3): The majority of the bed is massive with only a faint stratification at its top. Geochemically, the zeolite bed is very rich in SiO_2 and shows high Ba contents (Table 1).

The same zeolite bed has been detected by percussion coring at the northern margin of the central basin, SE of Ehingen (Figure 1). A clinoptilolite-heulandite bed was previously mentioned at this locality from material excavated in a construction pit (Wolff, 1974). Our re-investigation at this locality revealed the presence of a 15 cm thick clinoptilolite-heulandite bed at 4 m depth, that is at 424 m a.s.l., intercalated between aragonite-bearing laminites. Here, the aragonitic component could be identified as being formed by elongated fecal pellets (80–90 µm diameter; 400–650 µm length), probably produced by the brine shrimp *Artemia* (Jankowski, 1981). The mineralogical and geochemical composition of the bed, including a graded base with biotite crystals, is identical to the clinoptilolite-heulandite bed at the Wallerstein B25 underpass (Table 1).

Pink, euhedral, intact zircon crystals of 125–275 µm in size, extracted from the zeolite bed at Wallerstein B 25, revealed a 14.20 ± 0.08 Ma concordant U-Pb age (Table 2). This age is undistinguishable from that of the Harsány ignimbrite, a rhyolithic tuff of the Bükkalja Volcanic Field in Hungary (Lukács et al., 2015, 2018) and a bentonite bed located 53 km southeast of the Ries crater in the North Alpine Foreland Basin (Table 2; Text S3 and Data Set S2). In contrast, all other Cenozoic volcanic fields in Europe (Hegau and Urach, Kaiserstuhl, Eifel, Eger Rift, Vogelsberg and Hessian Depression, Massif Central) differ in chemistry and age (e.g.,

Wörner et al., 1986; Wedepohl, 2000; for review see; Lustrino & Wilson, 2007) from the investigated samples. Therefore, the Ries zeolite bed is interpreted to be a distal volcanic ash from the Bükkalja Volcanic Field in the Pannonian Basin, 760 km east of the Nördlinger Ries crater, and equivalent to one of the bentonite horizons in the Northern Alpine Foreland Basin (NAFB), specifically that of Unterzell (Table 1).

Previous geochemical analysis by Unger et al. (1990) suggested that volcanism in the Pannonian Basin was the source of the NAFB bentonites, and also recently Lukács et al. (2018) suggested a correlation with the Bükkalja Volcanic Field pyroclastics based on U-Pb zircon data. However, none of the recently dated NAFB bentonites (U-Pb dating by CA-ID-TIMS; Rocholl, Schaltegger, et al., 2018) revealed an identical age to the Unterzell bentonite investigated in this paper (U-Pb dating by LA-ICP-MS; Table 2), certainly reflecting the higher accuracy of the chemical abrasion (CA-ID-TIMS) method.

4.2. Stratigraphic Correlation From Surface to Depth

A re-inspection of drill cores NR 1001, NR 1003 and Nördlingen 1973 revealed a volcanic ash-derived bed at 192–218 m core depth, within the deeper part of the laminite member (Figure 4). Similar to its equivalents in the surface outcrops, the bed is intercalated within laminated organic-rich calcareous mudstones characterized by abundant aragonitic brine shrimp fecal pellets, typical of the analcime submember (Jankowski, 1981). However, in the drill samples the bed consists of K-NH_4-feldspar (buddingtonite; Table 1), a diagenetic successor derived from zeolites during burial and microbial ammonification in organic-rich sediments (Ramseyer et al., 1993). Geochemically, the bed is SiO_2-rich, as is the zeolite precursor, but contains K^+ and NH_4^+ instead of Ba^{2+} (Table 1). Based on the correlation of this volcanic-ash-derived silicate bed from marginal surface outcrops at 440–424 m a.s.l. to basin center drillings at 236-206 m a.s.l., a bowl-shaped crater fill geometry becomes evident (Figure 5), with the laminite member cropping out at the central basin margin, and younger crater fill units confined to drilling samples from the middle of the central basin.

4.3. Concentric Outcrop Pattern

The compilation and interpretation of drill data and exposures demonstrate that the surface outcrop of sedimentary crater fill members can be traced in a concentric pattern (Figure 6, Data Set S5):

(i) The basal member is readily identifiable in drilling samples, although the temporal relation to basin margin conglomerates and sandstones remains unclear. However, the latter commonly predate bioherms and travertines of later lake stages, and are slightly inclined toward the basin center. Therefore, they largely correspond to an early phase of basin development

(ii) The laminite member crops out in a broad fringe at the periphery of the central basin and in subbasins of the megablock zone. Temporary surface exposures show a 3°–10° inclination toward the basin center, with only one slump-related exception (Figure 6, Data Set S5). Bituminous shales intercalated in the basal parts of this member (i.e., at more than 245 m core depth in the basin center), crop out at the outermost margin of the central Ries plain (localities Wengenhausen, Nördlingen-Freibad, Goldberg, Ehingen). Basin-margin equivalents of the laminite member consist of early algal bioherms, and tufa mounds ("travertines"), which formed predominantly subaqueously in a soda lake environment, as determined from the characteristic sickle-cell-like shrinkage void fabric (Arp et al., 1998, 2010). Similarly, specific biogenic components in the tufa mounds, such as brine shrimp fecal pellets and dragon fly larvae, are known only from intervals of the laminite member (Dehm et al., 1977).

(iii) The marl member shows only a limited number of unequivocal surface outcrops (Hollaus, 1969) located at northern-central Ries. However, drillings demonstrate that this member can be traced as an ~500 m-wide circular strip in the central basin. Some of the basin-margin algal bioherms (e.g., at Adlersberg; Arp et al., 2013) may be equivalent to this unit.

(iv) Drilling samples and temporary exposures demonstrate that the clay member is restricted to the inner part of central Ries plain (Deffner & Fraas, 1877; Kranz, 1952). Basin margin equivalents are probably late algal bioherms (e.g., at Hainsfarth; Arp et al., 2013) and relict occurrences of oolites and freshwater limestones at hills near the crater rim.

Table 1
Mineralogical and Geochemical Composition of the Volcanic-Ash-Derived Zeolite-Feldspar Bed in the Miocene Ries Crater Lake Sediments and Reference Samples

Location	Sample number	Depth (m bs)	Altitude (m asl)	Mineral phases [a] XRD (semiquant. wt%)	C_{org} (wt%)	C_{carb} (wt%)	N_{tot} (wt%)	S_{tot} (wt%)
Wallerstein B25 underpass 2015	Wal-B25 C	0.83	439.2	Cpt (52), Hul (43), Mag (3), Qz (2)	0.02	<0.003	0.011	0.002
Wallerstein B25 underpass 2015	Wal-B25 B	0.84	439.2	Cpt (57), Hul (38), Mag (3), Qz (1)	0.02	<0.003	0.010	0.002
Wallerstein B25 underpass 2015	Wal-B25 A	0.94	439.1	Cpt (45), Hul (29), Pl (9), Sme (8), Bt (2)	0.03	<0.003	0.009	0.256
Ehingen-SE percussion drill core 2015	Eh 11	4.01	424.0	Cpt (54), Hul (20), Gth (16), Ilt (6)	0.09	0.007	0.010	0.028
Ehingen-SE percussion drill core 2015	Eh 12	4.08	423.9	Cpt (57), Hul (30), Gth (4), Ilt (4)	0.03	0.007	0.009	0.008
Ehingen-SE percussion drill core 2015	Eh 13	4.14	423.9	Cpt (31), Hul (17), Ilt (16), Sme (14)	0.32	0.65	0.034	0.260
Ehingen-SE percussion drill core 2015	Eh 14	4.15	423.9	n.a.	0.03	0.01	0.008	0.463
Ehinger Bach 1969 (sample Wolff)	EhB	0.0	424.0	Cpt (60), Hul (35), Mag (3), Qz (2)	0.10	0.16	0.024	0.005
drill core Nördlingen 1973	Noe1973-71	218.5	208.6	Bud, Kfs, Ab, Qz	1.57	0.06	2.642	0.040
drill core Nördlinger Ries 1001	Noe1001-1	206.7	213.4	Bud, Kfs, Ab, Qz	1.57	<0.003	1.970	0.139
drill core Nördlinger Ries 1003	Noe1003-82	192.7	236.4	Bud, Kfs, Ab	0.37	<0.003	2.460	0.211
bentonite Ammersberg, Northern Alpine Foreland Basin	AM2	8.0	485	n.a.	0.01	0.01	0.008	<0.002
bentonite Unterzell, Northern Alpine Foreland Basin	UZ1	7.0	499	n.a.	0.01	0.01	0.011	<0.002
bentonite Unterzell, Northern Alpine Foreland Basin	UZ2	7.0	499	n.a.	0.01	0.02	0.007	<0.002
Laacher See Tuff, Bringberg, 14 km S of Göttingen	LST	0.0	193	Qz (47), Clc (27), Bt (19), Mag (6)	0.27	<0.003	0.027	0.008
Tibolddaróc, Harsány Ignimbrit Unit, layer A [b]	Td-A = DX 46			n.a.	n.a.	n.a.	n.a.	n.a.

Table 1
Continued

LOI (wt%)	Sum oxides (wt%)	SiO_2 (wt%)	TiO_2 (wt%)	Al_2O_3 (wt%)	MnO (wt%)	MgO (wt%)	CaO (wt%)	Na_2O (wt%)	K_2O (wt%)	P_2O_5 (wt%)	Fe_2O_3 (wt%)	Ba (ppm)	Sr (ppm)
16.0	82.8	63.58	0.14	12.84	0.00	1.22	3.65	0.47	0.56	0.01	0.35	9,164	2,475
15.9	82.9	63.93	0.17	12.71	0.00	1.18	3.56	0.44	0.69	0.01	0.22	10,272	2,033
15.8	83.1	60.37	0.20	14.14	0.01	1.23	3.48	0.91	0.78	0.02	2.01	7,246	2,968
29.4	69.7	44.42	0.20	10.89	0.02	0.78	2.23	0.17	1.11	0.03	9.83	6,972	1,755
14.8	84.2	61.44	0.20	14.96	0.01	1.14	3.2	0.34	1.48	0.03	1.44	6,743	2,778
16.3	82.1	51.88	0.63	16.11	0.04	1.47	4.93	0.49	1.84	0.06	4.66	13,733	1,835
15.6	80.0	53.49	1.11	18.99	0.01	0.73	2.41	0.76	1.30	0.03	1.19	41,605	2,675
17.3	81.6	59.85	0.15	13.44	0.00	1.06	3.91	0.36	1.50	0.03	1.29	8,803	1906
10.4	89.5	60.26	0.03	17.38	0.02	0.80	0.84	0.53	5.75	0.28	3.65	135	372
8.7	91.3	60.15	0.03	17.19	0.02	0.87	0.73	0.44	7.85	0.35	3.64	144	464
25.1	74.8	51.52	0.01	14.77	0.02	0.10	0.13	0.23	6.69	0.14	1.24	160	42
18.9	81.1	50.9	0.29	19.60	0.02	2.72	1.48	0.17	0.98	0.05	4.87	168	43
17.6	82.4	56.0	0.31	15.84	0.03	3.55	1.56	0.15	1.34	0.05	3.56	201	60
19.9	80.0	53.0	0.21	16.98	0.02	3.11	1.43	0.1	0.73	0.03	4.44	150	48
13.1	86.8	50.6	0.30	21.76	0.47	0.49	1.02	5.47	3.75	0.05	2.85	1,353	88
3.6	97.5	73.826	0.15	12.99	0.04	0.15	1.35	2.72	4.75	0.04	1.48	901	98

n.a., not analyzed; b.d.l., below detection limit.
[a]Mineral name abbreviations according to Whitney and Evans (2010), except for Buddingtonite (Bud). [b]Average bulk composition of pumice clasts, data published in Lukács et al. (2007, 2015).

5. Discussion

5.1. Water Depth, Compaction and Crater Floor Sagging

Using the volcanic ash layer as an unequivocal temporal marker bed, the brine-shrimp-pellet-rich lower parts of the laminite member can be traced from 177 to 227 m a.s.l. (i.e., 200–250 m core depth) to the surface outcrop Wallerstein B 25 at 440 m a.s.l. without any lateral change in facies. A further correlation with the soda lake stage tufa mounds at the crystalline ring (Wallerstein mound with *Artemia*-pellet-rich interval at 465–470 m a.s.l.) results in a present-day height difference of 248–293 m.

However, the calculated compaction of coarse-grained siliciclastics (suevite-derived sandstones) and laminites below the ash layer can only account for 73 +49/-23 m subsidence. Corresponding stratigraphic backstripping of the ash layer (from today 209 m a.s.l. to initially 282 +49/-23 m a.s.l.) would result in a water depth of 184 +23/−49 m, i.e. the difference between the littoral equivalents (here: Wallerstein mound basal beds at 465 m a.s.l.) and the decompacted position of the buddingtonite bed (281 +49/−23 m a.s.l.) (Figure 5; Data Set S3). This high water depth, however, is inconsistent with previous sedimentological and paleontological interpretations suggesting a continuously shallow Ries lake of less than 10 m (Gall & Jung, 1979; von der Brelie, 1977; Weber, 1941). Only for the uppermost laminite/lowermost marl member Schauderna (1983) inferred intermittent maximum depths greater than 50 m. A re-evaluation of arguments indeed points to water depths generally shallower than 50 m for the volcanic-ash-containing laminate unit, as follows:

(i) Mud cracks were observed at the top of the basal member (272.55 m core depth: Jankowski, 1981) and within the laminite member (233.1 and 136.8 m core depth: Gall et al., 1974). These observations were interpreted as evidence for temporary subaerial exposure, and therefore shallow water depths. Our own observations in the NR 1003 core, however, revealed mud cracks only within the basal member (at 243.15, 242.95 and 242.7 m depth), and subaerial exposure with associated brecciation not until deposition of the marl member (less than 87 m core depth), suggesting a permanent water body at the time of the volcanic ash deposition.

(ii) Based on diatom associations, Schauderna (1983) suggested shallow water depths for most parts of the Nördlingen 1973 drill core. A closer look at the data of the volcanic-ash-containing analcime submember, however, shows that only few diatom assemblages are present, and all of them are dominated by planktonic species (samples at 205.4 and 218.4 m core depth with 95%–97% *Stephanodiscus binderanus*). While Schauderna (1983) considers the diatom-poor laminites as shallow water deposits emplaced during periods of increased salinity, the intercalated planktonic assemblages are interpreted to represent temporary highstands, with low-salinity waters of possibly 50 m depths.

(iii) Stable isotope analysis point to successive evaporation of the initial freshwater lake to a salt lake, with a salinity maximum during the laminite member (Füchtbauer et al., 1977; Jankowski, 1981; Rothe & Hoefs, 1977).

(iv) Likewise, the biomarker paleosalinity proxies methylated 2-methyl-2-[4′,8′,12′-trimethyltridecyl] chromans and isoprenoid thiophene ratio suggest that the volcanic ash bearing laminite sequence was deposited under mesohaline to hypersaline conditions (Barakat & Rullkötter, 1997).

Table 2
Single Zircon U-Pb Ages of Ries Crater Volcanic-Ash-Derived Zeolite Bed, Its Equivalent in the Northern Alpine Foreland Basin, and Its Source Area in the Pannonian Basin

	Ries crater	Northern alpine foreland basin	Pannonian basin
Locality	Wallerstein B25	Unterzell	Harsány ignimbrite
Sample ID	DX-73	DX-74	DX-46
n_{total}	65	36	120
n_{OLT}*	62	27	115
$n_{conc95-105}$**	45	13	39
Concordance age (Ma)	14.20	14.16	14.27
±2s	0.08	0.13	0.09
MSWD	1.3	1.4	1.2

* Passing outlier Tests; without pre-miocene xenocrystals.
** Data with Less than 5% Discordance.

While the data from points (i) and (ii) indicate a permanent water body with maximum depths of about 50 m, the high salinities inferred from points (iii) isotopes, and (iv) biomarkers, exclude higher water depths (of 180–190 m). Hence, we conclude that the observed bowl-shaped geometry of the sedimentary deposit fill can only be explained by an additional, significant subsidence of the crater floor, that is, a longer-term crater-floor sagging and subsidence.

Notably, prior to the identification of the Nördlinger Ries as an impact structure by Shoemaker and Chao (1961), several authors speculated on the possibility of syn- to post-sedimentary crater floor subsidence

(Dorn, 1940, 1942a, 1942b, 1942c, 1943; Koken, 1902; Weber, 1941; and finally, including, Walter Kranz (Kranz, 1952: "settling of blasting debris"), who was the advocate of the phreatomagmatic "blast theory" for the Ries formation; Kranz, 1911, 1912). In a similar manner, significant crater floor subsidence has been suggested for the 22 Ma Haughton impact structure, based on a 3°–3.5° inward dip of post-impact lacustrine strata (Hickey et al., 1988).

With respect to the duration of the crater floor sagging, an estimate can be made on the basis of the alternation of normal and reverse polarity sediment intervals measured at the Nördlingen 1973 drill core (Pohl, 1977): The volcanic ash layer (14.20 ± 0.08 Ma), embedded in sediment of normal polarity, corresponds to magnetochron C5ADn (14.609–14.163 Ma; ATNTS 2012: Gradstein et al., 2012). Given that, the following laminated sediments between 180 and 130 m core depth, with reverse polarity, correspond to C5ACr (14.163–14.070 Ma), while top parts of laminite member (between 130 and 111 m), the marl (111-52 m) and the clay member (52-0 m) correspond to C5ACn (14.070-13.739 Ma) and possibly even younger magnetochrons. Geologic evidence indicates that the clay member (i.e., the most recent lake sediments) accumulated on an almost stabilized crater floor, with its position and geometry explainable solely by conventional sediment compaction alone (exemplified for the *Cypridopsis* bed of the clay member: see Data Set S3). This implies that that the crater floor sagging did not stop until several 100 ka after the volcanic ash deposition.

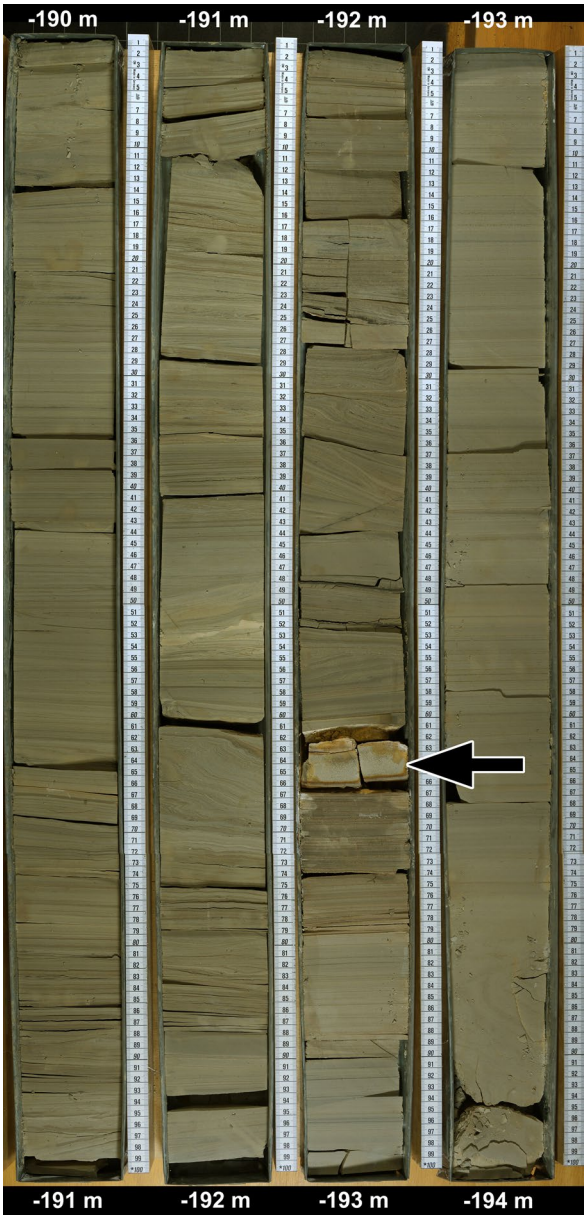

Figure 4. Volcanic-ash derived buddingtonite bed (arrow) in the laminite member at 192.61–192.66 m core depth, drilling NR 1003.

5.2. Synthesis of Evidence for Timing and Magnitude of Nördlinger Ries Crater Sedimentary Floor Filling, Sagging and Subsidence

In the case of the Ries crater, the impact occurred ~14.8 Ma ago, in the Middle Miocene, in a water-saturated landscape with water-containing target rocks and moist ambient atmospheric conditions. Interior crater sedimentation began with the immediate collapse of the impact vapor cloud, inducing catastrophic sedimentation in the crater interior and formation of the graded unit (Füchtbauer et al., 1977; Jankowski, 1977b; Stöffler et al., 2013). This was followed by a longer-term stepwise flooding due to 1) groundwater seepage (travertines and tufa mounds), and 2) fluvial tributaries from the rim and walls of the crater, together leading to a period of sedimentation lasting 1–2 Ma. At ~14.2 Ma, during the period of laminite unit deposition, the 14 cm thick volcanic ash layer was emplaced when the crater lake water depth was less than ~50 m (Figure 5).

Taken together, the comparison of 1) the water depth at the time of ash emplacement, 2) the thickness of sub-ash lake sediments, 3) the estimated amount of lake sediment compaction, and 4) post-ash emplacement subsidence, show that a significant amount of non-sediment-compaction-related basin subsidence occurred during an approximately 0.6 Myr-long period following crater formation and continued for several 100 kyr after the ash emplacement (Figures 5 and 6). We now turn to an examination of the causative factors that might be responsible for the documented 134 +23/−49 m crater floor subsidence unaccounted for by sediment compaction.

5.3. Causes of Impact Crater Post-Formation Floor Subsidence and Implications for Ries Crater

Detailed analysis of Earth and planetary impact craters and modeling of crater formation and evolution (Gault & Heitowitz, 1963; Gault et al., 1968; Melosh, 1989; Stöffler et al., 2006) have shown that there are several sources of positive and negative volume changes in the cra-

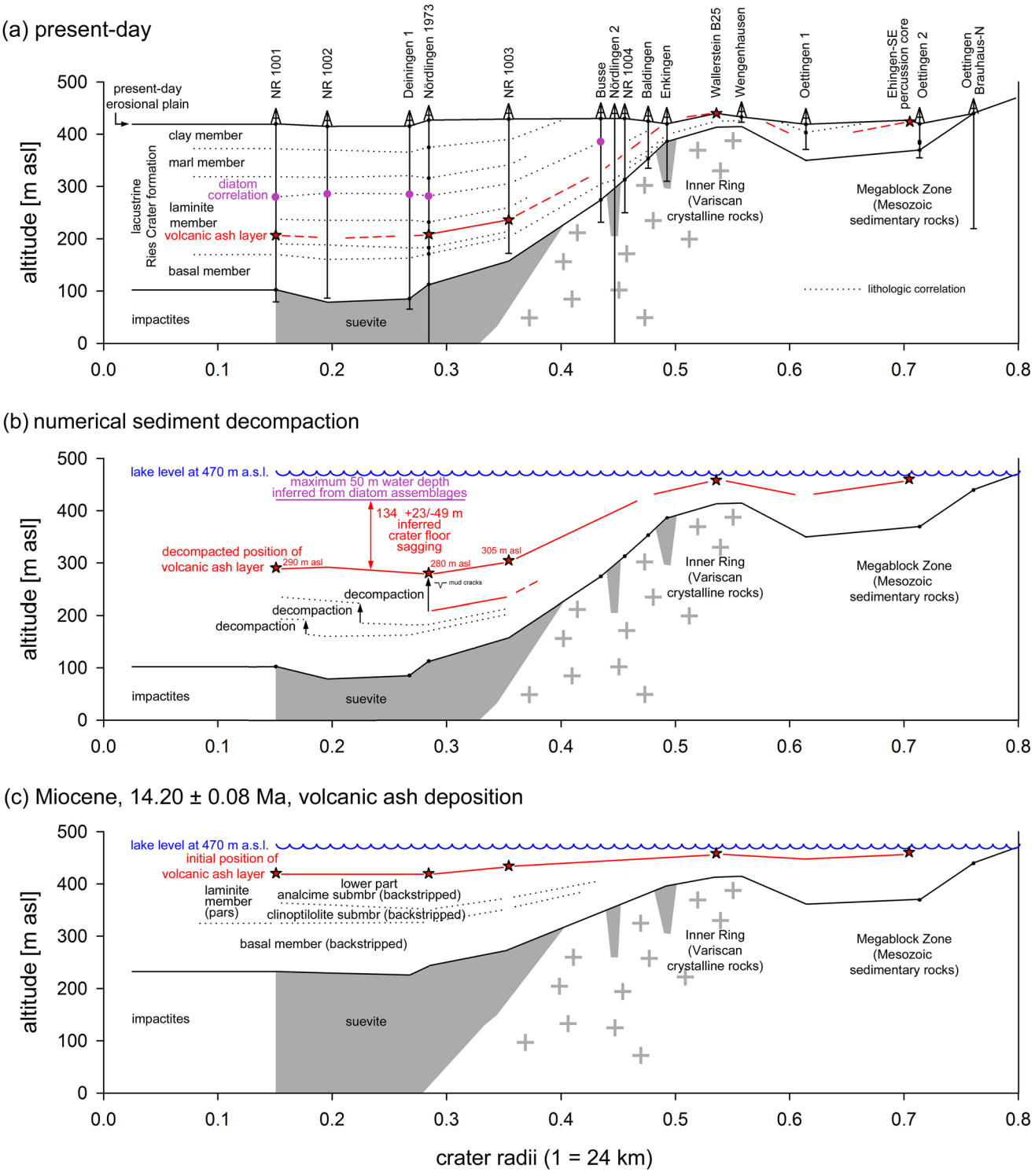

Figure 5. Schematic section through the Ries impact basin, with drilling locations arranged according to distance from crater center. (a) Present-day situation. (b) Numerical sediment decompaction. (c) Initial situation at the time of the volcanic ash deposition.

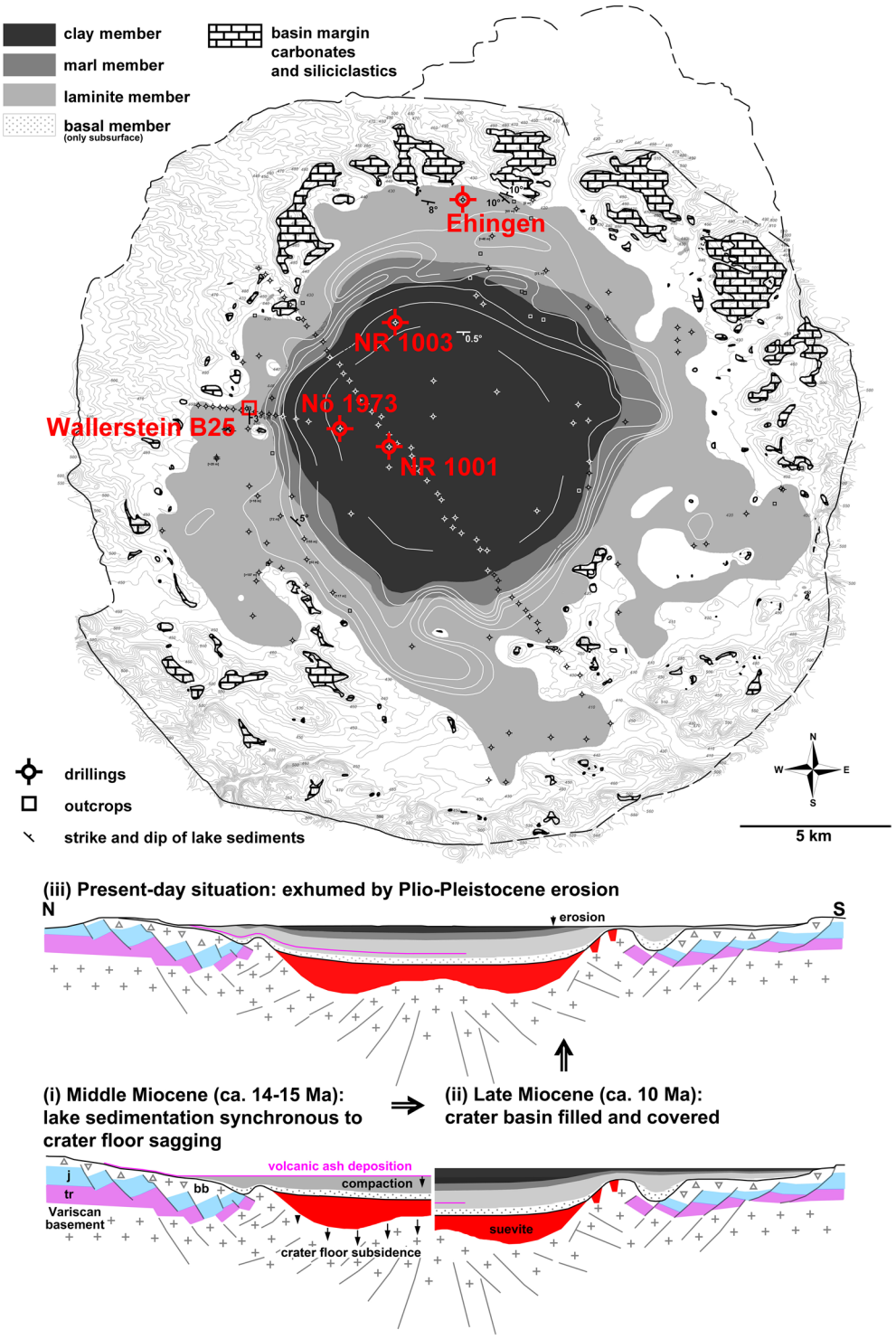

Figure 6. Geological map of the Ries impact crater fill showing the concentric outcrop of major lithofacies units and reconstruction of the evolution of the crater fill geometry. Miocene sediment thickness contour lines according to Ernstson (1974), with modifications according to drill data. tr, Triassic; j, Jurassic; bb, Bunte Breccia. (i) Initial situation at the time of the volcanic ash deposition. (ii) Situation at the end of the Miocene when the crater basin was completely filled. (iii) Present-day situation after Plio- to Pleistocene erosion of about 100 m sediment. General structure of the Ries basin modified from Pohl et al. (1977).

ter interior that can lead to vertical modification of the crater floor elevation (e.g., sagging, subsidence, and uplift). In the very short-term modification-stage of the cratering event, the transient crater cavity undergoes collapse; in smaller craters, rim crest/crater wall landsliding and floor uplift occur, and in larger craters, listric faulting, wall terracing, central peak formation, and general crater floor uplift and flattening are seen (see, e.g., Kenkmann et al., 2013). Additional contributions to crater floor shallowing include impact ejecta fallback and flow of impact melt down the crater wall and terraces, ponding on the crater floor (Hawke & Head, 1977; Melosh, 1989). Following this initial *rapid modification stage of the cratering event* itself, there are five types of processes that can cause additional changes in crater floor elevation.

1) *Thermal contraction processes*: Heat is imparted to the crater interior through the transfer of the kinetic energy of the impactor to the materials of the substrate, causing an array of effects ranging from mineral deformation to bulk impact melting. The magnitude of these processes scale with the velocity and mass of the projectile. Basin-scale impacts on the Moon such as ~930-km-diameter Orientale basin are characterized by huge, kilometers-deep impact melt seas in basin interiors. There the cooling and solidification can involve ~10% contraction, and extend for many hundreds of thousands of years, and cause many hundreds of meters of floor subsidence (e.g., Vaughan & Head, 2014; Vaughan et al., 2013).

The relatively small size of the Ries crater and the dispersal of impact melted material in the suevite deposit, suggest that subsidence due to thermal contraction of impact melt is negligible. A second source of thermal contraction is the conductive and radiative cooling of heat a) broadly distributed in the shocked and ejected material, and b) brought to the near-surface environment by the uplifting of deeper geotherms by the removal of cooler, near-surface material from the cavity and collapse of the transient cavity during the rapid modification stage. The magnitudes of these processes are scale- and substrate-dependent. For basin-scale events such as the Orientale Basin, these effects can contribute to thermal contraction and minor changes in basin topography lasting several tens of millions of years (e.g., Bratt, Solomon, & Head, 1985; Bratt, Solomon, Head, & Thurber 1985). The relatively small size of the Ries crater and the shallower geothermal gradient of the cooler continental lithosphere target substrate indicate that these processes produced negligible changes in floor topography.

2) *Viscous relaxation processes*: Lateral variations in geothermal gradient and lithospheric thickness, and temporal variations related to planetary thermal evolution, have been shown to be important in the evolution of impact basin topography on the Moon due to viscous relaxation processes over millions of years (e.g., Solomon et al., 1982). The small size of the Ries and the continental thermal structure of its substrate indicate that viscous relaxation processes were negligible.
3) *Closure of impact-induced fractures, faults, and mega-porosity induced by dilatancy*: During an impact event, the radial shock and attendant rarefaction waves cause significant downward and outward movement and displacement of the substrate, major shear deformation, and injection of impact melt and breccia dikes into the basement rock. Broadly referred to as *dilatancy* (inelastic volume increase due to intense deformation), such processes result in the near-instantaneous increase of the porosity of the autochthonous mega-breccias in the substrate below the crater interior and in the allochthonous breccia lenses deposited on the crater floor. Numerical simulations of impact-induced dilatancy point to significant subcrater porosities, decreasing with depth from more than 16% to less than 0.1% depending on crater size, structure, and hard rock quality (Collins, 2014). For example, Gohn et al. (2008) noted changes in post-impact marine sediment accommodation due to differential compaction of impact-generated materials in Chesapeake impact structure. Recent high-resolution lunar gravity data have further demonstrated its importance for the Moon (e.g., Soderblom et al., 2015). Although also scale-dependent, production of substrate porosity by impact-induced dilatancy, and its subsequent loss, is likely to be an important part of the topographic evolution of all crater interiors, including the Ries.
4) *Longer-term geologic modification processes*: Impact crater landforms are produced instantaneously in geologic time, are out-of-equilibrium with the ambient environment, and undergo modification by a range of geologic processes that influence the topography of the basin interior. On the Moon, magmatic processes involve volcanic flooding of crater interiors, (e.g., Whitten & Head, 2013) and intrusion of sills in the breccia lens below the crater floor causing uplift (e.g. Jozwiak, et al., 2015; Wilson & Head, 2018),

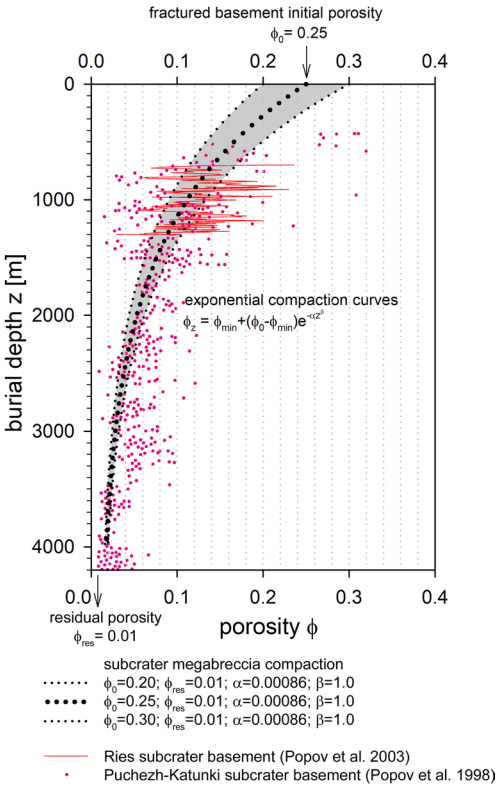

Figure 7. Model compaction curves of the subcrater crystalline rock breccias to demonstrate the plausibility of 134 +23/−49 m crater floor subsidence in the Ries impact structure.

both processes resulting in crater floor shallowing. Explosive volcanic eruptions on Mars are known to produce widely dispersed tephra (e.g., Kerber et al., 2012) and potentially significant deposits on crater floors (e.g., Le Deit et al., 2013). With the exception of the deposition of the distal ash layer, magmatic processes are not known to have influenced the evolution of the Ries crater.

Sedimentary infilling processes, however, have been significant in shallowing of the Ries crater floor. Numerous studies have demonstrated the role of fluvial, lacustrine and biological processes in the production, transport and deposition of sediment onto the crater floor. Conglomerates and stream deposits at the basin margins testify to the role of fluvial processes operating to modify the crater rim and walls, and to transport suspended sediment to the basin interior. Lacustrine deposits and sedimentary facies in the crater interior demonstrate that shallowing took place by infilling with lake sediments, aided by groundwater-related tufa deposition and local algal bioherm growth. No evidence for extensive eolian deposition (e.g., subaerial cross-bedding, etc.) has been documented. Thus, fluvial and lacustrine sedimentary infilling appear to be the dominant processes in crater floor shallowing of the Ries.

5) *Loading, flexure, compaction, and floor subsidence*: A potentially important factor in crater floor subsidence is the loading of the crater interior and the changes in topography induced by these loads and their effects. At very large impact basin scales, loading of the basin interior by dense volcanic lavas has been shown to induce flexure and significant subsidence in lunar basins (e.g., Solomon & Head, 1980), a factor that appears negligible at smaller crater scales.

In the case of the Ries crater, sediments deposited in the lacustrine environment will undergo internal volume changes related to compaction, dewatering and diagenesis, factors discussed in Section 5.1 (Data Set S3). Indeed, sediment load causing compaction is known to modify impact craters (Gohn et al., 2008; Tsikalas & Faleide, 2007; Tsikalas et al., 1998). In addition, the combination of the increasing sediment load and the oscillating water load (changes in depth with time) can exert pressure on the deeper substrate below the crater floor, and contribute to the closing of the dilatancy-induced mega-porosity in the underlying brecciated substrate.

In summary, of the range of processes operating to alter the interior topography of impact craters, the three most likely to be operating in the Ries crater are: 1) crater lake sedimentary infilling to reduce the depth of the floor, 2) dewatering and diagenesis of these lake sediments to increase the depth of the floor and 3) compaction of the dilatancy-induced mega-porosity in the breccia lens below the crater floor, to increase the depth of the floor. The deposition of the volcanic ash layer provides the opportunity to assess the magnitude and temporal relationships of these processes.

While a major part of the sagging in the Ries structure is to be assumed for the more than 4 km deep impact brecciated crystalline basement, crater floor sagging should also be evident by a convex surface of the 300 m thick suevite, which itself largely retained its high initial porosity (Förstner et al., 1967: 28%; Stöffler et al., 2013: 25%–30%; Popov et al., 2014: high-temperature suevite 27.9 ± 3.7%, and low-temperature suevite 21.4 ± 4.2%) due to its early lithification. Indeed, the few drillings available at the central crater inner slope are consistent with a convex shape of the suvite layer, although more drill cores are required for a final proof. As a consequence of the bowl-shaped crater fill geometry, Plio-Pleistocene exhumation and erosion lead to a circular outcrop pattern of the subsided lithostratigraphic units of the Ries impact crater fill, with bituminous shales and laminites at the margin, massive marlstones following farther inside, and a central area with lignite-bearing clays (Figure 6).

5.4. Estimation of Ries Subcrater Compaction

On the basis of the available data described here, our reconstruction indicates that the 134 +23/−49 m floor subsidence unaccounted for by lake sediment compaction is most plausibly attributable to early sediment-water loading and closure of sub-crater floor macro-porosity initially induced by impact-generated dilatancy. The exact initial geometry of the subcrater dilatant zone is unknown, but on the basis of the inferred geometry of the transient cavity, Stöffler et al. (2013) estimated a depth of ∼4 km for impact-induced fractures.

Unlike on the Moon, impact structures on Earth generally show a negative Bouguer gravity anomaly and reduced seismic velocities of the target basement, indicating an increased porosity relative to the unaffected surroundings (Milbury et al., 2015; Pilkington & Grieve, 1992). This also applies to the Ries impact structure, with a present negative Bouguer gravity anomaly (0–18 mgal in the crater interior: Kahle, 1969; Pohl et al., 1977) reflecting both the lower density sedimentary fill and residual porosity in the sub-crater brecciated rocks.

Initial porosities of subcrater megabreccias (i.e., porosities shortly after an impact event) are, to our knowledge, unknown. Polymict crystalline rock breccias of the inner ring of the Ries, which underwent lateral transport and retained their initial porosities due to early carbonate cementation, show macroporosities of up to 30% (Data Set S4). While this value is probably higher than for monomictic breccias and fractured blocks of the subcrater, it may represent an upper limit for initial porosity estimates ϕ_0. Direct measurements of present-day subcrater porosities, in turn, are known from few deep drilling sites, specifically at the Puchezh-Katunki, the Chesapeake, and the Ries (Popov et al., 1998, 2003, 2014). Further data are available for example, from the peak ring of the Chicxulub crater, whose fractured granitoids, however, were subject to lateral transport (Christeson et al., 2018; Elbra & Pesonen, 2011; Rae et al., 2019).

For the Ries impact structure, the 600 m cored subcrater lithologies consist of crystalline rocks (gneiss and granites, with additional amphibolites in upper part) with intercalated breccia dikes show highly variable porosities (0.0%–37.9%; Popov et al., 2003: their Table 3), even within the same target lithology. However, most core intervals show porosities ranging between ca. 5% and 18% (Popov et al., 2003: their Figure 11), providing a rough calibration for the 700–1300 m depth interval (i.e. 100 m eroded sediment added) of a subcrater compaction curve (Figure 7). For greater depth, porosity information of impact affected crystalline basement rocks is available from the 5,374 m deep borehole Vorotilovo of the Puchezh-Katunki impact structure: Porosities decrease from about 10%–20% at 600 m depth, to 5%–10% at 2,000 m depth, and finally about 2%–4% at 5,000 m depth (Popov et al., 1998, 2014). This 80-km-sized impact structure, however, is larger than the Ries, with brecciation and fracturing ranging deeper into the target basement rocks. We therefore assume low porosities of 2%–4% already at 2.5–3.5 km depth for the Ries subcrater rocks.

Based on these assumptions, a decompaction with an initial porosity ϕ_0 of 25% at $z = 0$ m, $\phi_z = 11\%$ for $z = 1{,}000$ m, and $\phi_z = 3\%$ for $z = 3{,}000$ m, would be consistent with 153 m long-term crater floor sagging (+37/−34 m for $\phi_0 = 20\%$–30%) (Figure 7; Data Set S4). While these calculations are preliminary and vary dependent on the assumptions made, they demonstrate that a mechanical compaction of brecciated subcrater crystalline rocks is in the range of the inferred 134 +23/−59 m crater floor subsidence. In any case, a further investigation of subcrater porosity evolution and potential other mechanisms of crater floor subsidence is required. Likewise, the microporosity of impact-affected rocks (e.g., Huber et al., 2021) is not taken into account in the present considerations.

5.5. Implications for Craters on Earth and Other Planetary Bodies

Clearly, initial dilatancy-related sub-crater porosity will vary as a function of a wide range of factors: impact event scale, substrate composition and structure, angle of impact, planetary gravity, presence nature and ambient state of an atmosphere and hydrosphere (e.g., Collins, 2014). Detailed documentation of the timing and likely origins of crater subsidence in the Ries crater provide a baseline for comparison to other craters on Earth and other planetary bodies.

For other craters on Earth, the relationship between crater interior subsidence and the application of loads from lake water and sediments should be assessed in detail. Does subsidence require the application of

these loads, or are there examples of significant subsidence occurring prior to lake formation and sedimentary infilling? On the Earth's Moon, low gravity and overburden pressure favor development of more significant dilatancy-related porosity and the lack of an atmosphere and hydrosphere precludes loading by lake water and lacustrine sediments; thus, the Moon is an excellent laboratory for the exploration of the variable parameter space in dilatancy-related porosity formation (e.g., Soderblom et al., 2015) and its long-term behavior. On Venus, crater floor subsidence has only been described for bright-floored (volcanism-free, lacking sedimentary infill) large impact craters, where a subsidence of 100–300 m is interpreted to reflect thermal subsidence of an insufficiently rigid, thin lithosphere (Brown & Grimm, 1996).

Mars, on the other hand, retains abundant impact craters, and was characterized early in its history by a thicker atmosphere and evidence for pluvial, fluvial and lacustrine activity and environments. An increasing number of Martian craters are known to contain sedimentary deposits (e.g., Eberswalde, Gale, Holden, Jezero: Ehlmann et al., 2008; Malin & Edgett, 2000; Schon et al., 2012; Tikhonravov, Antoniadi, Cassini: Fassett & Head, 2008a). Specifically, more than 400 open and closed crater lake basins of the Noachian and Hesperian era contain post-impact sediments of deltaic or lacustrine origin (Goudge et al., 2016), when Mars was at least intermittently warm and wet (Carr & Head, 2010a, 2010b). In addition, a number of areas in the northern lowlands (e.g., Utopia Planitia) show evidence of circular deformation and subsidence features that have been interpreted to represent impact craters that have been filled with sediment that underwent compaction and caused some related faulting (e.g., Buczkowski & Cooke, 2004; Buczkowski & McGill, 2002; Buczkowski et al., 2005; McGill & Hills, 1992).

There are currently no examples known of Martian craters that unequivocally show lacustrine strata inclined to the crater center. Rather, the evident and likely sedimentary crater fills are flat lying or inclined in various directions reflecting foreset beds (e.g., Terby: Ansan et al., 2011; Wilson et al., 2007) or possibly eolian, anticompensational deposition (Kite et al., 2016). At central mound in Gale Crater, strata dip gently (1.7°–4.5°) away from the central peak (Kite et al., 2013, 2016) toward a ring moat, explained by compaction due to later sediment load (Grotzinger et al., 2015). However, the low density of the sediments exposed at the current erosional crater bottom suggest that the 5 km deep crater was never filled completely with sediments, with a maximum sediment overburden of less than 1800 m (+600/−500 m) (Lewis et al., 2019). Likewise, modeling demonstrates that the observed sediment layer orientations in Gale could only be explained by $a > 3$ km thick donut-shaped past overburden, whose formation appears difficult to explain by known sedimentary processes (Gabasova & Kite, 2018). In any case, wherever clear concentric outcrop pattern of layered deposits in Martian craters were observed (e.g. unnamed crater within Schiaparelli basin: PSP_005897_1790; Beyer et al., 2012; unnamed crater in West Arabia Terra: MOC M14-01647; Malin & Edgett, 2000; Crommelin Crater: Lewis et al., 2008), these layered deposits are rather regional deposits (possibly duststones) draping over various, partially eroded craters (Grotzinger & Milliken, 2012; Lewis et al., 2008). On the other hand, Buczkowski and Cooke (2004) and Buczkowski et al. (2005) mapped circular graben in Utopia Planitia, and concluded that graben spacing supported the fill and compaction of wet sediment of up to 1–2 km thickness (assuming that the underlying basement was rigid and that all the compaction was in the sediment infill). In a more recent analysis, Gabasova and Kite (2018) updated approaches to the analyses of sediment compaction, but also assumed that the basement underwent no compaction. Unfortunately, details of the subsurface sediment bed orientation, the presence of any temporal marker beds, and the duration of the modification process are unknown for most of these studies.

The apparent absence of crater floor sagging of exposed beds on Mars may reflect either a lack of observations, or the possibility that many Martian impacts might have occurred during cold and dry phases (no rainfall, fluvial erosion or lacustrine environments), no significant groundwater influx, and volatile-rich but frozen icy regolith). In this case, flooding and sedimentation occur a significant time after crater formation, perhaps during intermittent wet phases. Such a scenario might be consistent with the proposed short intermittent formation time of deltaic systems in Martian crater basins (de Villiers et al., 2013). For Gale crater, the inclination of present-day surface beds may not necessarily reflect compaction of hidden strata beneath (with an estimated thickness of 1–2 km; Grotzinger et al., 2015), but may partially result from sagging in the impact-fractured subsurface. On the other hand, Buczkowski et al. (2005) and Gabasova and Kite (2018) have shown evidence for sediment filled craters that have undergone differential compaction, under the assumption that the sub-sediment basement was rigid and non-porous. On the basis of the Ries

crater example documented here, future analysis and exploration should investigate the temporal relationships between initial crater formation and the role of subsequent flooding and water-sediment flooding on crater floor subsidence.

6. Conclusions

(i) The clinoptilolite-heulandite-buddingtonite bed in the lacustrine succession of Ries impact crater is a distal volcanic ash of the contemporaneous, intensive volcanism in the Pannonian Basin, 760 km east of the Ries
(ii) This volcanic ash bed can be traced from surface outcrops at the basin margin to 220 m depth within the basin center, thereby demonstrating a deeply bowl-shaped geometry and concentric outcrop pattern of the sedimentary crater fill
(iii) The compaction of sedimentary units alone is insufficient to explain this geometry which we thus attribute to water-sediment loading and closure of dilatancy-induced mega-porosity in the underlying breccia lens
(iv) These results have important implications for understanding the nature and history of impact craters on the Earth and other planetary bodies, particularly Mars

Data Availability Statement

All data used in this publication are available in Arp et al. (2021) on the Göttingen Research Online Data repository.

Acknowledgments
The authors acknowledge †Michael Wolff who first mentioned the clinoptilolite bed in the Ries impact structure and provided a corresponding sample (Ehingen locality) for the present study. The authors are indebted to Exxon Mobil Production Deutschland GmbH for access to drillings NR 1001–1004, sampling permit, and permission for publication of data. Karin Heck, Ries Crater Museum, supported sampling and documentation in the drill core facilities. The study benefited from a number of drill core and outcrop samples provided by Terrasond GmbH Günzburg, Geotechnik Augsburg Ingenieurgesellschaft mbH, Oliver Sachs, Kurt Kroepelin, Ralf Barfeld and Gisela Pösges. Percussion drill coring was carried out by Steffen Stark, LfU Hof. XRF analyses were performed by Gerald Hartmann. The authors thank Andreas Murr and Gerhard Doppler for NAFB bentonite reference samples. The authors are grateful to Joanna Morgan, Richard Grieve, and Fred Horz for information on impactite porosities. This work was funded by German Research Foundation, grant DFG AR335/9-1. L. Zeng thanks the China Scholarship Council (CSC) for his financial support. R. Lukács is funded by the Bolyai J. Research Fellowship. The authors thank M. H. Poelchau and an anonymous reviewer for their detailed, constructive, and very helpful comments and suggestions that significantly improved the manuscript. Finally, we acknowledge support by the Open Access Publication Funds of the Georg-August-University Göttingen. Open access funding enabled and organized by Projekt DEAL.

References

Ansan, V., Loizeau, D., Mangold, N., Le Mouélic, S., Carter, J., Poulet, F., et al. (2011). Stratigraphy, mineralogy, and origin of layered deposits inside Terby crater, Mars. *Icarus*, *211*(1), 273–304. https://doi.org/10.1016/j.icarus.2010.09.011

Arp, G., Bissett, A., Brinkmann, N., Cousin, S., de Beer, D., Friedl, T., et al. (2010). Tufa-forming biofilms of German karstwater streams: Microorganisms, exopolymers, hydrochemistry, and calcification. *Geological Society, London, Special Publications*. *336*, 83–118. https://doi.org/10.1144/SP336.6

Arp, G., Blumenberg, M., Hansen, B. T., Jung, D., Kolepka, C., Lenz, O., et al. (2013). Chemical and ecological evolution of the Miocene Ries impact crater lake, Germany: A reinterpretation based on the Enkingen (SUBO 18) drill core. *The Geological Society of America Bulletin*, *125*(7–8), 1125–1145. https://doi.org/10.1130/B30731.1

Arp, G., Dunkl, I., Jung, D., Karius, V., Lukács, R., Zeng, L. et al (2021). Data and Supporting Information for publication 'A volcanic ash layer in the Nördlinger Ries impact structure (Miocene, Germany): Indication of crater fill geometry and origins of long-term crater floor sagging'. *Göttingen Research Online Data*. https://doi.org/10.25625/DRPFR9

Arp, G., Hofmann, J., & Reitner, J. (1998). Microbial fabric formation in spring mounds ("microbialites") of alkaline salt lakes in the Badain Jaran sand sea, PR China. *Palaios*, *13*(6), 581–592. https://doi.org/10.2307/3515349

Artemieva, N. A., Wünnemann, K., Krien, F., Reimold, W. U., & Stöffler, D. (2013). Ries crater and suevite revisited—Observations and modeling Part II: Modeling. *Meteorit Planetary Science*, *48*(4), 590–627. https://doi.org/10.1111/maps.12085

Athy, L. F. (1930). Density, porosity, and compaction of sedimentary rocks. *American Association of Petroleum Geologists Bulletin*, *14*(1), 1–24.

Barakat, A. O., & Rullkötter, J. (1997). A comparative study of molecular paleosalinity indicators: Chromans, tocopherols and C_{20} isoprenoid thiophenes in Miocene lake sediments (Nördlinger Ries, Southern Germany). *Aquatic Geochemistry*, *3*(2), 169–190. https://doi.org/10.1023/A:1009645510876

Beard, D. C., & Weyl, P. K. (1973). Influence of texture on porosity and permeability of unconsolidated sand. *American Association of Petroleum Geologists Bulletin*, *57*, 349–369. https://doi.org/10.1306/819A4272-16C5-11D7-8645000102C1865D

Beyer, R. R., Stack, K. M., Griffes, J. L., Milliken, R. E., Herkenhoff, K. E., Byrne, S., et al. (2012). An atlas of mars sedimentary rocks as seen by HIRISE. In J. P. Grotzinger, & R. E. Milliken (Eds.), *Sedimentary geology of Mars. SEPM special publication* (Vol. 102, pp. 49–95). Tulsa, OK: SEPM.

Bolten, R., Gall, H., & Jung, W. (1976). Die obermiozäne (sarmatische) Fossil-Lagerstätte Wemding im Nördlinger Ries (Bayern). Ein Beitrag zur Charakterisierung des Riessee-Biotops. *Geologische Blätter für Nordost-Bayern*, *26*, 75–94.

Bratt, S. R., Solomon, S. C., & Head, J. W. (1985). The evolution of impact basins: Cooling, subsidence, and thermal stress. *Journal of Geophysical Research*, *90*, 12415–12433. https://doi.org/10.1029/jb090ib14p12415

Bratt, S. R., Solomon, S. C., Head, J. W., & Thurber, C. H. (1985). The deep structure of lunar basins: Implications for basin formation and modification. *Journal of Geophysical Research*, *90*, 3049–3064. https://doi.org/10.1029/jb090ib04p03049

Brown, C. D., & Grimm, R. E. (1996). Floor subsidence and rebound of large Venus craters. *Journal of Geophysical Research*, *101*(E11), 26057–26067. https://doi.org/10.1029/96JE02706

Buczkowski, D. L., & Cooke, M. L. (2004). Formation of double-ring circular grabens due to volumetric compaction over buried impact craters: Implications for thickness and nature of cover material in Utopia Planitia, Mars. *Journal of Geophysical Research*, *109*(E2), E02006. https://doi.org/10.1029/2003JE002144

Buczkowski, D. L., Frey, H. V., Roark, J. H., & McGill, G. E. (2005). Buried impact craters: A topographic analysis of quasi-circular depressions, Utopia basin, Mars. *Journal of Geophysical Research*, *110*, E03007. https://doi.org/10.1029/2004JE002324

Buczkowski, D. L., & McGill, G. E. (2002). Topography within circular grabens: Implications for polygon origin, Utopia Planitia, Mars. *Geophysical Research Letters*, *29*, 1155. https://doi.org/10.1029/2001GL014100

Carr, M. H., & Head, J. W., III (2010a). Acquisition and history of water on Mars. In N. A. Cabrol, & E. A. Grin (Eds.), *Lakes on Mars* (pp. 31–67). Amsterdam: Elsevier.

Carr, M. H., & Head, J. W., III (2010b). Geologic history of Mars. *Earth and Planetary Science Letters*, *294*(3–4), 185–203. https://doi.org/10.1016/j.epsl.2009.06.042

Christeson, G. L., Gulick, S. P. S., Morgan, J. V., Gebhardt, C., Kring, D. A., Le Ber, E., et al. (2018). Extraordinary rocks from the peak ring of the Chicxulub impact crater: *P*-wave velocity, density, and porosity measurements from IODP/ICDP Expedition 364. *Earth and Planetary Science Letters*, *495*, 1–11. https://doi.org/10.1016/j.epsl.2018.05.013

Collins, G. S. (2014). Numerical simulations of impact crater formation with dilatancy. *Journal of Geophysical Research: Planets*, *119*(12), 2600–2619. https://doi.org/10.1002/2014JE004708

Craddock, R. A., & Howard, A. D. (2002). The case for rainfall on a warm, wet early Mars. *Journal of Geophysical Research: Planets*, *107*(E11), 5111. https://doi.org/10.1029/2001JE001505.5111

Deffner, C., & Fraas, O. (1877). *Begleitworte zur geognostischen Spezialkarte von Württemberg. Atlasblätter Bopfingen und Ellenberg (Explanatory notes on the geognostic special map of Wuerttemberg. Sheets Bopfingen and Ellenberg; in German)*. Stuttgart: Kohlhammer.

Dehm, R., Gall, H., Höfling, R., Jung, W., & Malz, H. (1977). Die Tier- und Pflanzenreste aus den obermiozänen Riessee-Ablagerungen in der Forschungsbohrung Nördlingen 1973 (Animal and plant remains from the Upper Miocene Rieslake deposits of the research drilling Nördlingen 1973; in German). *Geologica Bavarica*, *75*, 91–109.

Deit, L. L., Hauber, E., Fueten, F., Pondrelli, M., Rossi, A. P., & Jaumann, R. (2013). Sequence of infilling events in Gale Crater, Mars: Results from morphology, stratigraphy, and mineralogy. *Journal of Geophysical Research: Planets*, *118*, 2439–2473. https://doi.org/10.1002/2012JE004322

de Villiers, G., Kleinhans, M. G., & Postma, G. (2013). Experimental delta formation in crater lakes and implications for interpretation of Martian deltas. *Journal of Geophysical Research: Planets*, *118*(4), 651–670. https://doi.org/10.1002/jgre.20069

Dorn, C. (1940). Beiträge zur Kenntnis der tertiären Ablagerungen des östlichen Vorrieses im Monheimer Gebiet (Contributions to the knowledge of the Tertiary deposits of the eastern Ries periphery in the Monheim area; in German). *Neues Jahrbuch für Mineralogie, Geologie und Paläontologie Beilage-Band*. *84* (Abt. B), 129–176.

Dorn, C. (1942a). Beiträge zur Geologie des Rieses I (Contributions to the geology of the Ries I; in German). *Zentralblatt für Mineralogie, Geologie und Paläontologie, Abt. B Geologie und Paläontologie*. 1942, 105–116, 145–159, 161–187.

Dorn, C. (1942b). Beiträge zur Geologie des Rieses II (Contributions to the geology of the Ries II; in German). *Zentralblatt für Mineralogie, Geologie und Paläontologie, Abt. B Geologie und Paläontologie*, 311–348.

Dorn, C. (1942c). Beiträge zur Geologie des Rieses (Contributions to the geology of the Ries; in German). *Neues Jahrbuch für Mineralogie, Geologie und Paläontologie Beilage-Band*, *86*(Abt. B), 390–449).

Dorn, C. (1943). Beiträge zur Geologie des Rieses (Contributions to the geology of the Ries; in German). Neues Jahrbuch für Mineralogie, Geologie und Paläontologie Monatshefte, 1943(Abt. B), 299–312).

Ehlmann, B. L., Mustard, J. F., Fassett, C. I., Schon, S. C., Head, J. W., Des Marais, D. J., et al., & CRISM team. (2008). Clay minerals in delta deposits and organic preservation potential on Mars. *Nature Geoscience*, *1*, 355–358. https://doi.org/10.1038/ngeo207

Einsele, G. (2000). Mechanical and chemical diagenesis. In G. Einsele (Ed.), *Sedimentary basins. Evolution, facies, and sediment budget* (2nd ed., pp. 647–705). Berlin: Springer.

Elbra, T., & Pesonen, L. J. (2011). Physical properties of the Yaxcopoil-1 deep drill core, Chicxulub impact structure, Mexico. *Meteoritics & Planetary Sciences*, *46*(11), 1640–1652. https://doi.org/10.1111/j.1945-5100.2011.01253.x

Engelhardt, W. (1997). Suevite breccia of the Ries impact crater, Germany: Petrography, chemistry and shock metamorphism of crystalline rock clasts. *Meteoritics & Planetary Sciences*, *32*, 545–554. https://doi.org/10.1111/j.1945-5100.1997.tb01299.x

Ernstson, K. (1974). The structure of the Ries crater from geoelectric depth soundings. *Journal of Geophysics*, *40*, 639–659.

Fassett, C. I., & Head, J. W. (2008a). Valley network-fed, open-basin lakes on Mars: Distribution and implications for Noachian surface and subsurface hydrology. *Icarus*, *198*, 37–56. https://doi.org/10.1016/j.icarus.2008.06.016

Fassett, C. I., & Head, J. W. (2008b). The timing of Martian valley network activity: Constraints from buffered crater counting. *Icarus*, *195*, 61–89. https://doi.org/10.1016/j.icarus.2007.12.009

Förstner, U. (1967). Petrographische Untersuchungen des Suevit aus den Bohrungen Deiningen und Wörnitzostheim im Ries von Nördlingen (Petrographic investigations of suevite from the drillings Deiningen and Wörnitzostheim in the Ries of Nördlingen; in German). *Contributions to Mineralogy and Petrology*, *15*, 281–308. https://doi.org/10.1007/BF00404198

Füchtbauer, H., von der Brelie, G., Dehm, R., Förstner, U., Gall, H., Höfling, R., et al. (1977). Tertiary lake sediments of the Ries, research borehole Nördlingen 1973—A summary. *Geologica Bavarica*, *75*, 13–19.

Gabasova, L. R., & Kite, E. S. (2018). Compaction and sedimentary basin analysis on Mars. *Planetary and Space Science*, *152*, 86–106. https://doi.org/10.1016/j.pss.2017.12.021

Gall, H., & Jung, W. (1979). Zur Genese der jungtertiären Fossil-Lagerstätte Wemding im Nördlinger Ries (Bayern) (On the genesis of the Late Tertiary Lagerstätte Wemding in the Nördlinger Ries (Bavaria); in German). *Geologische Blätter für Nordost-Bayern*, *29*, 12–25.

Gall, H., Jung, W., & Dehm, R. (1974). Vorbericht über die Tier- und Pflanzenreste aus den obermiozänen Riessee-Ablagerungen in der Forschungsbohrung Nördlingen 1973 (Preliminary report on the animal and plant remains from the Upper Miocene Rieslake deposits of the research drilling Nördlingen 1973; in German). *Geologica Bavarica*, *72*, 53–57.

Gault, D. E., & Heitowitz, B. D. (1963). The partition of energy for hypervelocity impact craters formed in rock. *Proceedings of the sixth Hypervelocity Impact Symposium*, 2, 419–456).

Gault, D. E., Quaide, W. L., & Oberbeck, V. R. (1968). Impact cratering mechanics and structures. In B. M. French, & N. M. Short (Eds.), *Shock metamorphism in natural materials* (pp. 87–99). Baltimore, MD: Mono Book Corp.

Gohn, G. S., Koeberl, C., Miller, K. G., Reimold, W. U., Browning, J. V., Cockell, C. S., et al. (2008). Deep drilling into the Chesapeake Bay impact structure. *Science*, *320*(5884), 1740–1745. https://doi.org/10.1126/science.1158708

Goudge, T. A., Aureli, K. L., Head, J. W., III, Fassett, C. I., & Mustard, J. F. (2015). Classification and analysis of candidate impact crater-hosted closed-basin lakes on Mars. *Icarus*, *260*, 346–367. https://doi.org/10.1016/j.icarus.2015.07.026

Goudge, T. A., Fassett, C. I., Head, J. W., Mustard, J. F., & Aureli, K. L. (2016). Insights into surface runoff on early Mars from Paleolake basin morphology and stratigraphy. *Geology*, *44*(6), 419–422. https://doi.org/10.1130/G37734.1

Gradstein, F. M., Ogg, J. G., Schmitz, M. D., & Ogg, G. M. (2012). *The geologic time scale 2012* (p. 1144). Amsterdam: Elsevier.

Grotzinger, J. P., Gupta, S., Malin, M. C., Rubin, D. M., Schieber, J., Siebach, K., et al. (2015). Deposition, exhumation, and paleoclimate of an ancient lake deposit, Gale crater, Mars. *Science*, *350*(6257), aac7575-1–aac7575–12. https://doi.org/10.1126/science.aac7575

Grotzinger, J. P., & Milliken, R. E. (2012). The sedimentary rock record of Mars: Distribution, origins and global stratigraphy. In J. P. Grotzinger, & R. E. Milliken (Eds.), *Sedimentary geology of Mars. SEPM special publication* (Vol. 102, pp. 1–48). Tulsa, OK: SEPM.

Gurov, E. P., Kelley, S. P., Koeberl, C., & Dykan, N. I. (2006). Sediments and impact rocks filling the Boltysh impact crater. In C. S. Cockell, C. Koeberl, & I. Gilmour (Eds.), *Biological processes associated with impact events. Impact Studies* (Vol. 8, pp. 335–358). Heidelberg: Springer.

Guyard, H., St-Onge, G., Pienitz, R., Francus, P., Zolitschka, B., Clarke, G. K. C., et al. (2011). New insights into Late Pleistocene glacial and postglacial history of northernmost Ungava (Canada) from Pingualuit Crater Lake sediments. *Quaternary Science Reviews*, *30*, 3892–3907. https://doi.org/10.1016/j.quascirev.2011.10.002

Hawke, B. R., & Head, J. W. (1977). Impact melt in lunar crater interiors. In D. J. Roddy, R. O. Pepin, & R. B. Merrill (Eds.), *Impact and explosion cratering* (p. 815). New York, NY: Pergamon Press.

Hickey, L. J., Johnson, K. R., & Dawson, M. R. (1988). The stratigraphy, sedimentology, and fossils of the Haughton formation: A post-impact crater-fill, Devon Island, NWT, Canada. *Meteoritics & Planetary Sciences*, *23*, 221–231. https://doi.org/10.1111/j.1945-5100.1988.tb01284.x

Hollaus, E. (1969). *Geologische Untersuchungen im Ries. Das Gebiet der Blätter Nördlingen-Ost und Nördlingen-West, mit besonderer Berücksichtigung der Pleistozän-Ablagerungen (Geological investigations in the Ries. The area of the sheets Nördlingen-East and Nördlingen-West, with special reference to the Pleistocene deposits; in German)* (p. 85). (doctoral thesis, Ludwig Maximilian University Munich).

Huber, M. S., Gulick, S. P. S., Tisato, N., Kovaleva, E., Clark, M., & Fourie, F. (2021). *Preliminary results of geophysical properties of granites taken from a transect through the Vredefort impact structure*. Paper presented at 52nd lunar and planetary science conference, The Woodlands, TX: Lunar and Planetary Institute.

Hüttner, R. (1969). Bunte Trümmermassen und Suevit (Varicolored sedimentary ejecta and suevite). *Geologica Bavarica*, *61*, 142–200.

Hüttner, R., & Schmidt-Kaler, H. (1999). Die Geologische Karte des Rieses 1:50 000 (2., überarbeitete Auflage). Erläuterungen zu Erdgeschichte, Bau und Entstehung des Kraters sowie zu den Impaktgesteinen (Geological map of the Ries 1:50 000 (2nd revised edition). Explanations of earth history, structure and formation of the crater and the impact rocks; in German). *Geologica Bavarica*, *104*, 7–76.

Irwin, R. P., Howard, A. D., Craddock, R. A., & Moore, J. M. (2005). An intense terminal epoch of widespread fluvial activity on early Mars: 2. Increased runoff and paleolake development. *Journal of Geophysical Research*, *110*, E12S15. https://doi.org/10.1029/2005JE002460

Jankowski, B. (1977a). Die Postimpakt-Sedimente in der Forschungsbohrung Nördlingen 1973 (The post-impact sediments in the research drilling Nördlingen 1973; in German). *Geologica Bavarica*, *75*, 21–36.

Jankowski, B. (1977b). The graded unit on top of the suevite layer in the borehole Nördlingen 1973. *Geologica Bavarica*, *75*, 155–162.

Jankowski, B. (1981). Die Geschichte der Sedimentation im Nördlinger Ries und Randecker Maar (The sedimentary history of the Nördlinger Ries and Randecker Maar; in German). *Bochumer Geologische und Geotechnische Arbeiten*, *6*, 1–315.

Jozwiak, L. M., Head, J. W., III, & Wilson, L. (2015). Lunar floor-fractured craters as magmatic intrusions: Geometry, modes of emplacement, associated tectonic and volcanic features, and implications for gravity anomalies. *Icarus*, *248*, 424–447. https://doi.org/10.1016/j.icarus.2014.10.052

Kahle, H. G. (1969). Abschätzung der Störungsmasse im Nördlinger Ries (Estimation of the disrupted mass in the Nördlinger Ries; in German). *Zeitschrift für Geophysik*, *35*, 317–345.

Kenkmann, T., Collins, G. S., & Wünnemann, K. (2013). The modification stage of crater formation. In G. R. Osinski, & E. Pierazzo (Eds.), *Impact cratering: Processes and products* (pp. 60–75). Oxford: Wiley-Blackwell.

Kerber, L., Head, J. W., III, Madeleine, J.-B., Forget, F., & Wilson, L. (2012). The dispersal of pyroclasts from ancient explosive volcanoes on Mars: Implications for the friable layered deposits. *Icarus*, *219*, 358–381. https://doi.org/10.1016/j.icarus.2012.03.016

Kite, E. S., Lewis, K. W., Lamb, M. P., Newman, C. E., & Richardson, M. I. (2013). Growth and form of the mound in Gale Crater, Mars: Slope wind enhanced erosion and transport. *Geology*, *41*(5), 543–546. https://doi.org/10.1130/G33909.1

Kite, E. S., Sneed, J., Mayer, D. P., Lewis, K. W., Michaels, T. I., Hore, A., & Rafkin, S. C. R. (2016). Evolution of major sedimentary mounds on Mars: Buildup via anticompensational stacking modulated by climate change. *Journal of Geophysical Research: Planets*, *121*(11), 2282–2324. https://doi.org/10.1002/2016JE005135

Koken, E. (1902). Geologische Studien im fränkischen Ries. Zweite Folge (Geological studies in the Franconian Ries. Second episode; in German). *Neues Jahrbuch für Mineralogie, Geologie und Paläontologie Beilage-Band*, 15, 422–472).

Kominz, M. A., & Pekar, S. F. (2001). Oligocene eustasy from two-dimensional sequence stratigraphic backstripping. *The Geological Society of America Bulletin*, *113*(3), 291–304. https://doi.org/10.1130/0016-7606(2001)113<0291:OEFTDS>2.0.CO;2

Kranz, W. (1911). Das Nördlinger Riesproblem. *Jahresberichte und Mitteilungen des Oberrheinischen Geologischen Vereins, Neue Folge*, *1*, 32–35. https://doi.org/10.1127/jmogv/1/1911/32

Kranz, W. (1912). Das Nördlinger Riesproblem II (The problem of the Nördlinger Ries II; in German). *Jahresberichte und Mitteilungen des Oberrheinischen Geologischen Vereins, Neue Folge*, *2*, 54–65.

Kranz, W. (1952). Die Braunkohlen im Nördlinger Riesbecken (Lignites in the Nördlinger Ries basin; in German). *Geologisches Jahrbuch*, *66*, 81–117.

Landmann, G., Reimer, A., Lemcke, G., & Kempe, S. (1996). Dating late glacial abrupt climate changes in the 14,570 yr long continuous varve record of Lake Van, Turkey. *Palaeogeography, Palaeoclimatology, Palaeoecology*, *122*, 107–118. https://doi.org/10.1016/0031-0182(95)00101-8

Lewis, K. W., Aharonson, O., Grotzinger, J. P., Kirk, R. L., McEwen, A. S., & Suer, T.-A. (2008). Quasi-periodic bedding in the sedimentary rock record of Mars. *Science*, *322*(5907), 1532–1535. https://doi.org/10.1126/science.1161870

Lewis, K. W., Peters, S., Gonter, K., Morrison, S., Schmerr, N., Vasavada, A. R., & Gabriel, T. (2019). A surface gravity traverse on Mars indicates low bedrock density at Gale crater. *Science*, *363*(6426), 535–537. https://doi.org/10.1126/science.aat0738

Lukács, R., Harangi, S., Bachmann, O., Guillong, M., Danišík, M., Buret, Y., et al. (2015). Zircon geochronology and geochemistry to constrain the youngest eruption events and magma evolution of the Mid-Miocene ignimbrite flare-up in the Pannonian Basin, eastern central Europe. *Contributions to Mineralogy and Petrology*, *170*, 52. https://doi.org/10.1007/s00410-015-1206-8

Lukács, R., Harangi, S., Guillong, M., Bachmann, O., Fodor, L., Buret, Y., et al. (2018). Early to Mid-Miocene syn-extensional massive silicic volcanism in the Pannonian basin (East-Central Europe): Eruption chronology, correlation potential and geodynamic implications. *Earth-Science Reviews*, *179*, 1–19. https://doi.org/10.1016/j.earscirev.2018.02.005

Lukács, R., Harangi, S., Ntaflos, T., Koller, F., & Pécskay, Z. (2007). A Bükkalján megjelenő felső riolittufaszint vizsgálati eredményei: a harsányi ignimbrit egység (The characteristics of the Upper Rhyolite Tuff Horizon in the Bükkalja Volcanic Field: The Harsány ignimbrite unit). *Foldtani Kozlony*, *137*(4), 487–514.

Lustrino, M., & Wilson, M. (2007). The Circum-Mediterranean anorogenic Cenozoic Igneous Province. *Earth-Science Reviews*, *81*(1–2), 1–65. https://doi.org/10.1016/j.earscirev.2006.09.002

Maillart, J. (1991). Differenciation entre tectonique synsedimentaire et compaction differentielle. *Memoires de sciences de la terre de l' Ecole des Mines de Paris*, *12*, 1–193.

Malin, M. C., & Edgett, K. S. (2000). Sedimentary rocks of early Mars. *Science*, *290*(5498), 1927–1937. https://doi.org/10.1126/science.290.5498.1927

McGill, G. E., & Hills, L. S. (1992). Origin of giant Martian polygons. *Journal of Geophysical Research*, *97*, 2633–2647. https://doi.org/10.1029/91je02863

Melles, M., Brigham-Grette, J., Minyuk, P. S., Nowaczyk, N. R., Wennrich, V., DeConto, R. M., et al. (2012). 2.8 Million years of arctic climate change from lake El'gygytgyn, NE Russia. *Science*, *337*(6092), 315–320. https://doi.org/10.1126/science.1222135

Melosh, H. J. (1989). Impact cratering: A geologic process. *Oxford Monographs on Geology and Geophysics Series*, *11*, 245.

Milbury, C., Johnson, B. C., Melosh, H. J., Collins, G. S., Blair, D. M., Soderblom, J. M., et al. (2015). Preimpact porosity controls the gravity signature of lunar craters. *Geophysical Research Letters*, *42*, 9711–9716. https://doi.org/10.1002/2015GL066198

Milliken, R. E., Grotzinger, J. P., & Thomson, B. J. (2010). Paleoclimate of Mars as captured by the stratigraphic record in Gale Crater. *Geophysical Research Letters*, *37*, L04201. https://doi.org/10.1029/2009GL041870

Osinski, G. R. (2004). Impact melt rocks from the Ries structure, Germany: An origin as impact melt flows?. *Earth and Planetary Science Letters*, *226*(3–4), 529–543. https://doi.org/10.1016/j.epsl.2004.08.012

Osinski, G. R. (2006). Effect of volatiles and target lithology on the generation and emplacement of impact crater fill and ejecta deposits on Mars. *Meteoritics & Planetary Sciences*, *41*(10), 1571–1586. https://doi.org/10.1111/j.1945-5100.2006.tb00436.x

Osinski, G. R., Lee, P., Spray, J. G., Parnell, J., Lim, D. S. S., Bunch, T. E., et al. (2005). Geological overview and cratering model for the Haughton impact structure, Devon Island, Canadian High Arctic. *Meteoritics & Planetary Sciences*, *40*(12), 1759–1776. https://doi.org/10.1111/j.1945-5100.2005.tb00145.x

Partridge, T. C., Kerr, S. J., Metcalfe, S. E., Scott, L., Talma, A. S., & Vogel, J. C. (1993). The Pretoria Saltpan: A 200,000 year Southern African lacustrine sequence. *Palaeogeography, Palaeoclimatology, Palaeoecology*, *101*(3–4), 317–337. https://doi.org/10.1016/0031-0182(93)90022-B

Pilkington, M., & Grieve, R. A. F. (1992). The geophysical signature of terrestrial impact craters. *Reviews of Geophysics*, *30*, 161–181. https://doi.org/10.1029/92RG00192

Pohl, J. (1977). Paläomagnetische und gesteinsmagnetische Untersuchungen an den Kernen der Forschungsbohrung Nördlingen 1973. *Geologica Bavarica*, *75*, 329–348.

Pohl, J., Stöffler, D., Gall, H., & Ernstson, K. (1977). The Ries impact crater. In D. J. Roddy, R. G. Pepin, & R. B. Merril (Eds.), *Impact and explosion cratering* (pp. 343–458). New York: Pergamon Press.

Popov, Y. A., Pimenov, V. P., Pevzner, L. A., Romushkevich, R. A., & Popov, E. Y. (1998). Geothermal characteristics of the Vorotilovo deep borehole drilled into the Puchezh-Katunk impact structure. *Tectonophysics*, *291*, 205–223. https://doi.org/10.1016/S0040-1951(98)00041-9

Popov, Y., Mayr, S., Romushkevich, R., Burkhardt, H., & Wilhelm, H. (2014). Comparison of petrophysical properties of impactites for four meteoritic impact structures. *Meteoritics & Planetary Sciences*, *49*, 896–920. https://doi.org/10.1111/maps.12299

Popov, Y., Pohl, J., Romushkevich, R., Tertychnyi, V., & Soffel, H. (2003). Geothermal characteristics of the Ries impact structure. *Geophysical Journal International*, *154*, 355–378. https://doi.org/10.1046/j.1365-246X.2003.01925.x

Rae, A. S. P., Collins, G. S., Morgan, J. V., Salge, T., Christeson, G. L., Leung, J., et al. (2019). Impact-Induced Porosity and Microfracturing at the Chicxulub Impact Structure. *Journal of Geophysical Research: Planets*, *124*, 1960–1978. https://doi.org/10.1029/2019JE005929

Ramseyer, K., Diamond, L. W., & Boles, J. R. (1993). Autigenic K-NH_4-feldspar in sandstones: A fingerprint of the diagenesis of organic matter. *Journal of Sedimentary Petrology*, *63*(6), 1092–1099. https://doi.org/10.1306/D4267CAD-2B26-11D7-8648000102C1865D

Reiff, W. (1977). The Steinheim Basin – an impact structure. In D. J. Roddy, R. G. Pepin, & R. B. Merril (Eds.), *Impact and explosion cratering* (pp. 309–320). New York, NY: Pergamon Press.

Reimer, A., Landmann, G., & Kempe, S. (2009). Lake Van, eastern Anatolia, hydrochemistry and history. *Aquatic Geochemistry*, *15*, 195–222. https://doi.org/10.1007/s10498-008-9049-9

Revil, A., Grauls, D., & Brévart, O. (2002). Mechanical compaction of sand/clay mixtures. *Journal of Geophysical Research*, *107*(B11), 11. https://doi.org/10.1029/2001JB000318

Rocholl, A., Böhme, M., Gilg, H. A., Pohl, J., Schaltegger, U., & Wijbrans, J. (2018). Comment on "A high-precision 40Ar/39Ar age for the Nördlinger Ries impact crater, Germany, and implications for the accurate dating of terrestrial impact events" by Schmieder et al. (Geochimica et Cosmochimica Acta 220 (2018) 146-157). *Geochimica et Cosmochimica Acta*, *238*, 599–601. https://doi.org/10.1016/j.gca.2018.05.018

Rocholl, A., Schaltegger, U., Gilg, H. A., Wijbrans, J., & Böhme, M. (2018). The age of volcanic tuffs from the upper Freshwater Molasse (North Alpine Foreland Basin) and their possible use for tephrostratigraphic correlations across Europe for the middle Miocene. *International Journal of Earth Sciences*, *107*(2), 387–407. https://doi.org/10.1007/s00531-017-1499-0

Rothe, P., & Hoefs, J. (1977). Isotopen-geochemische Untersuchungen an Karbonaten der Ries-See-Sedimente der Forschungbohrung Nördlingen 1973 (Isotope-geochemical investigation of carbonates of the Ries-lake-sediments of the research drilling Nördlingen 1973; in German). *Geologica Bavarica*, *75*, 59–66.

Schauderna, H. (1983). Die Diatomeenflora aus den miozänen Seeablagerungen im Nördlinger Ries (The diatom flora of the Miocene lake deposits of the Nördlinger Ries; in German). *Palaeontographica, B*, *188*, 83–193.

Schmieder, M., Kennedy, T., Jourdan, F., Buchner, E., & Reimold, W. U. (2018a). A high-precision 40Ar/39Ar age for the Nördlinger Ries impact crater, Germany, and implications for the accurate dating of terrestrial impact events. *Geochimica et Cosmochimica Acta*, *220*, 146–157. https://doi.org/10.1016/j.gca.2017.09.036

Schmieder, M., Kennedy, T., Jourdan, F., Buchner, E., & Reimold, W. U. (2018b). Response to comment on "A high-precision 40Ar/39Ar age for the Nördlinger Ries impact crater, Germany, and implications for the accurate dating of terrestrial impact events" by Schmieder et al. (Geochimica et Cosmochimica Acta 220 (2018) 146-157). *Geochimica et Cosmochimica Acta*, *238*, 602–605. https://doi.org/10.1016/j.gca.2018.07.025

Schon, S. C., Head, J. W., & Fassett, C. I. (2012). An overfilled lacustrine system and progradational delta in Jezero crater, Mars: Implications for Noachian climate. *Planetary and Space Science*, *67*, 28–45. https://doi.org/10.1016/j.pss.2012.02.003

Schröder, J., & Dehm, R. (1950). Geologische Untersuchungen im Ries. Das Gebiet des Blattes Harburg (Geological research in the Ries. The area of the sheet Harburg; in German). *Abhandlungen des Naturwissenschaftlichen Vereins für Schwaben e.V. in Augsburg*, 5, 1–147).

Sclater, J. G., & Christie, P. A. F. (1980). Continental stretching: An explanation of the post-mid-Cretaceous subsidence of the central North Sea basin. *Journal of Geophysical Research*, *85*(B7), 3711–3739. https://doi.org/10.1029/JB085iB07p03711

Shanahan, T. M., Overpeck, J. T., Anchukaitis, K. J., Beck, J. W., Cole, J. E., Dettman, D. L., et al. (2009). Atlantic forcing of persistent drought in west Africa. *Science*, *324*(5925), 377–380. https://doi.org/10.1126/science.1166352

Shoemaker, E. M., & Chao, E. C. T. (1961). New evidence for the impact origin of the Ries basin, Bavaria, Germany. *Journal of Geophysical Research*, *66*(10), 3371–3378. https://doi.org/10.1029/JZ066i010p03371

Siegert, S., Branney, M. J., & Hecht, L. (2017). Density current origin of a melt-bearing impact ejecta blanket (Ries suevite, Germany). *Geology*, *45*(9), 855–858. https://doi.org/10.1130/G39198.1

Siegert, S., & Hecht, L. (2019). Heterogeneity of melts in impact deposits and implications for their origin (Ries suevite, Germany). *Meteoritics & Planetary Sciences*, *54*(10), 2409–2447. https://doi.org/10.1111/maps.13210

Soderblom, J. M., Evans, A. J., Johnson, B. C., Melosh, H. J., Miljković, K., Phillips, R. J., et al. (2015). The fractured Moon: Production and saturation of porosity in the lunar highlands from impact cratering. *Geophysical Research Letters*, *42*, 6939–6944. https://doi.org/10.1002/2015GL065022

Solomon, S. C., Comer, R. P., & Head, J. W. (1982). The evolution of impact basins: Viscous relaxation of topographic relief. *Journal of Geophysical Research*, *87*, 3975–3992. https://doi.org/10.1029/jb087ib05p03975

Solomon, S. C., & Head, J. W. (1980). Lunar Mascon basins: Lava filling, tectonics, and evolution of the lithosphere. *Reviews of Geophysics*, *18*, 107–141. https://doi.org/10.1029/rg018i001p00107

Stockhecke, M., Sturm, M., Brunner, I., Schmincke, H. U., Sumita, M., Kipfer, R., et al. (2014). Sedimentary evolution and environmental history of Lake Van (Turkey) over the past 600,000 years. *Sedimentology*, *61*, 1830–1861. https://doi.org/10.1111/sed.12118

Stöffler, D., Artemieva, N. A., Wünnemann, K., Reimold, W. U., Jacob, J., Hansen, B. K., & Summerson, I. A. T. (2013). Ries crater and suevite revisited—Observations and modeling Part I: Observations. *Meteoritics & Planetary Sciences*, *48*, 515–589. https://doi.org/10.1111/maps.12086

Stöffler, D., Ryder, G., Ivanov, B. A., Artemieva, N. A., Cintala, M. J., & Grieve, R. A. F. (2006). Cratering history and lunar chronology. *Reviews in Mineralogy and Geochemistry*, *60*(1), 519–596. https://doi.org/10.2138/rmg.2006.60.05

Sturm, S., Wulf, G., Jung, D., & Kenkmann, T. (2013). The Ries impact, a double-layer rampart crater on Earth. *Geology*, *41*(5), 531–534. https://doi.org/10.1130/g33934.1

Talbot, M. R., & Johannessen, T. (1992). A high resolution paleoclimatic record for the last 27,500 years in tropical west Africa from the carbon and nitrogen isotopic composition of lacustrine organic matter. *Earth and Planetary Science Letters*, *110*(1–4), 23–37. https://doi.org/10.1016/0012-821X(92)90036-U

Tsikalas, F., & Faleide, J. I. (2007). Post-impact structural crater modification due to sediment loading: An overlooked process. *Meteoritics & Planetary Sciences*, *42*(11), 2013–2029. https://doi.org/10.1111/j.1945-5100.2007.tb00557.x

Tsikalas, F., Gudlaugsson, S. T., & Faleide, J. I. (1998). Collapse, infilling, and postimpact deformation at the Mjølnir impact structure, Barents Sea. *The Geological Society of America Bulletin*, *110*(5), 537–552. https://doi.org/10.1130/0016-7606(1998)110<0537:CIAPDA>2.3.CO;2

Unger, H. J., Fiest, W., & Niemeyer, A. (1990). Die Bentonite der ostbayerischen Molasse und ihre Beziehungen zu den Vulkaniten des Pannonischen Beckens (The bentonite of the East-Bavarian Molasse and their relation to the volcanic rocks of the Pannonian Basin; in German). *Geologisches Jahrbuch D*, *96*, 67–112.

Vaughan, W. M., & Head, J. W., III (2014). Impact melt differentiation in the south Pole-Aitken basin: Some observations and speculations. *Planetary and Space Science*, *91*, 101–106. https://doi.org/10.1016/j.pss.2013.11.010

Vaughan, W. M., Head, J. W., III, Wilson, L., & Hess, P. C. (2013). Geology and petrology of enormous volumes of impact melt on the Moon: A case study of the Orientale basin impact melt sea. *Icarus*, *223*, 749–765. https://doi.org/10.1016/j.icarus.2013.01.017

von der Brelie, G. (1977). Die Pollenflora der See-Sedimente in der Forschungsbohrung Nördlingen 1973 (The pollen flora of the lake sediments of the research drilling Nördlingen 1973; in German). *Geologica Bavarica*, *75*, 111–125.

Weber, E. (1941). Geologische Untersuchungen im Ries. Das Gebiet des Blattes Wemding (Geological research in the Ries. The area of the sheet Wemding; in German). *Abhandlungen des Naturkunde- und Tiergartenvereins für Schwaben e.V., 3 (geol.-paläont. Reihe, 2. Heft)*, 1–248.

Wedepohl, K. H. (2000). The composition and formation of Miocene tholeiites in the central European Cenozoic plume volcanism (CECV). *Contributions to Mineralogy and Petrology*, *140*(2), 180–189. https://doi.org/10.1007/s004100000184

Whitney, D. L., & Evans, B. W. (2010). Abbreviations for names of rock-forming minerals. *American Mineralogist*, *95*, 185–187. https://doi.org/10.2138/am.2010.3371185

Whitten, J. L., & Head, J. W., III (2013). Detecting volcanic resurfacing of heavily cratered terrain: Flooding simulations on the Moon using lunar orbiter laser altimeter (LOLA) data. *Planetary and Space Science*, *85*, 24–37. https://doi.org/10.1016/j.pss.2013.05.013

Wilson, L., & Head, J. W., III (2018). Lunar floor-fractured craters: Modes of dike and sill emplacement and implications of gas production and intrusion cooling on surface morphology and structure. *Icarus*, *305*, 105–122. https://doi.org/10.1016/j.icarus.2017.12.030

Wilson, S. A., Howard, A. D., Moore, J. M., & Grant, J. A. (2007). Geomorphic and stratigraphic analysis of Crater Terby and layered deposits north of Hellas Basin, Mars. *Journal of Geophysical Research*, *112*(8), E08009. https://doi.org/10.1029/2006JE002830

Wolff, M. (1974). *Limnische Kalke und Dolomite im Nördlinger Ries und Steinheimer Becken (Limnic limestones and dolomites of the Nördlinger Ries and Steinheim Basin; in German)* (p. 116+28). (doctoral thesis, Ruhr-University Bochum).

Wolff, M., & Füchtbauer, H. (1976). Die karbonatische Randfazies der tertiären Süßwasserseen des Nördlinger Ries und des Steinheimer Beckens (The calcareous marginal facies of the Tertiary freshwater lakes of the Nördlinger Ries and Steinheim Basin; in German). *Geologisches Jahrbuch, D*, *14*, 3–53.

Wolf, M. (1977). Kohlenpetrographische Untersuchung der See-Sedimente der Forschungsbohrung Nördlingen 1973 und Vergleich mit anderen Untersuchungsergebnissen aus dem Ries (Coal petrological investigation of the lake sediments of the research drilling Nördlingen 1973; in German). *Geologica Bavarica*, *75*, 127–138.

Wörner, G., Zindler, A., Staudigel, H., & Schmincke, H. U. (1986). Sr, Nd, and Pb isotope geochemistry of tertiary and quaternary volcanics from west Germany. *Earth and Planetary Science Letters*, *79*(1–2), 107–119. https://doi.org/10.1016/0012-821X(86)90044-0

References From the Supporting Information

Arp, G., Reimer, A., Simon, K., Sturm, S., Wilk, J., Kruppa, C., et al. (2019). The Erbisberg drilling 2011: Implications for the structure and post-impact evolution of the inner ring of the Ries impact crater. *Meteoritics & Planetary Sciences*, *54*(10), 2448–2482. https://doi.org/10.1111/maps.13293

Dunkl, I., Mikes, T., Simon, K., and von Eynatten, H. (2008), Brief introduction to the windows program Pepita: Data visualization, and reduction, outlier rejection, calculation of trace element ratios and concentrations from LA-ICP-MS data. In. In Sylvester, P. (Ed.) *Laser*

ablation ICP-MS in the Earth sciences: Current practices and outstanding issues, short course (Vol. 40, 334–340). Mineralogical Association of Canada.

Frei, D., & Gerdes, A. (2009). Precise and accurate in situ U-Pb dating of zircon with high sample throughput by automated LA-SF-ICP-MS. *Chemical Geology*, *261*, 261–270.

Jackson, S., Pearson, N., Griffin, W., & Belousova, E. (2004). The application of laser ablation inductively coupled plasma-mass spectrometry to in situ U-Pb zircon geochronology. *Chemical Geology*, *211*, 47–69.

Landmann, G. (1996). *Van See/Türkei: Sedimentologie, Warvenchronologie und Paläoklima der letzten 15,000 Jahre (Lake Van/Turkey: Sedimentology, warve chronology, and paleoclimate of the last 15000 years; in German)* (p. 123+13). (Doctoral thesis, University of Hamburg).

Ludwig, K. R. (2012). User's manual for isoplot 3.75: A geochronological toolkit for Microsoft excel. *Berkeley Geochronology Center Special Publication*. *4*, 70.

Marillo-Sialer, E., Woodhead, J., Hergt, J., Greig, A., Guillong, M., Gleadow, A., et al. (2014). The zircon "matrix effect": Evidence for an ablation rate control on the accuracy of U-Pb age determinations by LA-ICP-MS. *Journal of Analytical Atomic Spectrometry*, *29*(6), 981–989.

Paces, J. B., & Miller, J. D. (1993). Precise U-Pb ages of Duluth Complex and related mafic intrusions, northeastern Minnesota: geochronological insights into physical, petrogenetic, paleomagnetic and tectonomagmatic processes associated with the 1.1 Ga midcontinent rift system. *Journal of Geophysical Research*, *98*, 13997–14013.

Pupin, J. P. (1980). Zircon and granite petrology. *Contributions to Mineralogy and Petrology*, *73*, 207–220.

Sliwinski, J. T., Guillong, M., Liebske, C., Dunkl, I., von Quadt, A., & Bachmann, O. (2017). Improved accuracy of LA-ICP-MS U-Pb ages of Cenozoic zircons by alpha dose correction. *Chemical Geology*, *472*, 8–21.

Vermeesch, P. (2018). IsoplotR: A free and open toolbox for geochronology. *Geoscience Frontiers*, *9*, 1479–1493. https://doi.org/10.1016/j.gsf.2018.04.001

Wiedenbeck, M., Allé, P., Corfu, F., Griffin, W. L., Meier, M., Oberli, F., et al. (1995). Three natural zircon standards for U-Th-Pb, Lu-Hf, trace element and REE analyses. *Geostandards Newsletters*, *19*, 1–23.

Wotzlaw, J.-F., Schaltegger, U., Frick, D. A., Dungan, M. A., Gerdes, A., & Günther, D. (2013). Tracking the evolution of large-volume silicic magma reservoirs from assembly to supereruption. *Geology*, *41*, 867–870.